The structural repertoire of *Fusarium oxysporum* f. sp. *lycopersici* effectors revealed by experimental and computational studies

Daniel S. Yu[1], Megan A. Outram[1,§,*], Ashley Smith[1], Carl L. McCombe[1], Pravin B. Khambalkar[1], Sharmin A. Rima[1], Xizhe Sun[1,2,4], Lisong Ma[1,4], Daniel J. Ericsson[1,3], David A. Jones[1], Simon J. Williams[1,§]

[1]Research School of Biology, The Australian National University, Canberra, ACT 2601, Australia

[2]Key Laboratory of Hebei Province for Plant Physiology and Molecular Pathology, College of Life Sciences, Hebei Agriculture University, Baoding, China

[3]The Australian Nuclear Science and Technology Organisation, Australian Synchrotron, Clayton, Victoria 3168, Australia

[4]State Key Laboratory of North China Crop Improvement and Regulation, College of Horticulture, Hebei Agricultural University, Baoding 071001, China

[§]Corresponding author: Simon Williams; simon.williams@anu.edu.au, +61 2 6125 7862
Megan Outram: megan.outram@csiro.au

* Current address: Black Mountain Science and Innovation Park, CSIRO Agriculture and Food, Canberra, Australia

Keywords: Fungal effectors, FOLD, *Fusarium oxysporum*, Secreted in xylem (SIX) effectors, Structural biology

Funding: Australian Research Council (DP200100388, FT200100135, DE170101165). Australian Academy of Science (Thomas Davies Grant). Australian National University Future Scheme (35665). Australian Institute of Nuclear Science and Engineering.

29	Daniel S. Yu	0000-0003-0454-7989
30	Megan A Outram	0000-0003-4510-3575
31	Ashley Smith	
32	Carl L. McCombe	0000-0001-9347-8879
33	Pravin B. Khambalkar	0000-0003-3641-6553
34	Sharmin A. Rima	0000-0003-2808-8369
35	Xizhe Sun	
36	Lisong Ma	0000-0001-9288-869X
37	Daniel J. Ericsson	0000-0001-5101-9244
38	David A. Jones	0000-0001-8809-5822
39	Simon J. Williams	0000-0003-4781-6261

Abstract

Plant pathogens secrete proteins, known as effectors, that function in the apoplast or inside plant cells to promote virulence. Effector recognition by cell-surface or cytosolic receptors results in the activation of defence pathways and plant immunity. Despite their importance, our general understanding of fungal effector function and recognition by immunity receptors remains poor. One complication often associated with effectors is their high sequence diversity and lack of identifiable sequence motifs precluding prediction of structure or function. In recent years, several studies have demonstrated that fungal effectors can be grouped into structural classes, despite significant sequence variation and existence across taxonomic groups. Using protein x-ray crystallography, we identify a new structural class of effectors hidden within the secreted in xylem (SIX) effectors from *Fusarium oxysporum* f. sp. *lycopersici* (*Fol*). The recognised effectors Avr1 (SIX4) and Avr3 (SIX1) represent the founding members of the ***Fol*** **d**ual-domain (FOLD) effector class, with members containing two distinct domains. Using AlphaFold2, we predicted the full SIX effector repertoire of *Fol* and show that SIX6 and SIX13 are also FOLD effectors, which we validated experimentally for SIX6. Based on structural prediction and comparisons, we show that FOLD effectors are present within three divisions of fungi and are expanded in pathogens and symbionts. Further structural comparisons demonstrate that *Fol* secretes effectors that adopt a limited number of structural folds during infection of tomato. This analysis also revealed a structural relationship between transcriptionally co-regulated effector pairs. We make use of the Avr1 structure to understand its recognition by the I receptor, which leads to disease resistance in tomato. This study represents an important advance in our understanding of *Fol*-tomato, and by extension plant-fungal interactions, which will assist the development of novel control and engineering strategies to combat plant pathogens.

63 **Introduction**

64 *Fusarium oxysporum* is a soil-borne fungal pathogen responsible for destructive vascular wilt diseases
65 in a wide range of plants. It ranks within the top ten important fungal pathogens in terms of scientific
66 and economic importance [1]. The best-characterised *F. oxysporum* pathosystem involves *F.*
67 *oxysporum* f. sp. *lycopersici* (*Fol*) and tomato. Previous studies of *Fol*-infected tomato identified a
68 number of fungal proteins within the xylem sap [2]. These secreted in xylem (SIX) effector proteins
69 represent major pathogenicity determinants across different *formae speciales* of *F. oxysporum*.
70 Currently, 14 SIX effectors have been identified in *Fol* consisting of small (less than 300 amino acids in
71 length), secreted, cysteine-rich proteins [3-6]. Most SIX effectors are encoded on the conditionally-
72 dispensable chromosome 14 required for *Fol* pathogenicity [7]. This dispensable chromosome can be
73 horizontally transferred from *Fol* to a non-pathogenic strain of *F. oxysporum*, resulting in a transfer of
74 pathogenicity [4, 7]. To date, all 14 SIX effectors lack sequence identity with proteins of known
75 function, preventing prediction of function based on their amino acid sequence. Several SIX effectors
76 have been shown to be essential for full virulence including SIX1, SIX2, SIX3, SIX5 and SIX6 from *Fol* [5,
77 8-11], SIX1 from *F. oxysporum* f. sp. *conglutinans* (*Focn*), which infects cabbage [12], SIX4 from *F.*
78 *oxysporum* isolate Fo5176, which infects Arabidopsis [13], and SIX1 and SIX8 from *F. oxysporum* f. sp.
79 *cubense*, which infects banana [14, 15]. *Fol SIX3* (*Avr2*) and *SIX5* are adjacent, divergently-transcribed
80 genes with a common promoter, and SIX5 has been shown to interact with SIX3 to promote virulence
81 by enabling symplastic movement of SIX3 via plasmodesmata [16]. *Focn SIX8* and *PSE1* (pair with *SIX8*
82 1) are also a divergently-transcribed effector gene pair that function together to suppress phytoalexin
83 production and plant immunity in Arabidopsis [17]. In *Fol, SIX8* forms a similar gene pair with *PSL1*
84 (*PSE1*-like 1) [17]. Despite their roles in fungal pathogenicity, the virulence functions of most SIX
85 effectors remain unknown.

86 To combat pathogen attack, plants possess resistance genes that encode immunity receptors
87 capable of recognising specific effectors leading to disease resistance. Four resistance genes,
88 introgressed into tomato from related wild species, have been cloned. *I* and *I-7* encode
89 transmembrane receptor proteins containing extracellular leucine-rich repeat (LRR) domains and
90 short cytoplasmic domains (LRR-RPs) [18, 19]. *I-2* encodes a cytoplasmic receptor containing
91 nucleotide binding (NB) and C-terminal LRR domains [20], while *I-3* encodes a transmembrane protein
92 with an extracellular S-receptor-like domain and cytoplasmic serine/threonine kinase domain (SRLK)
93 [21]. *Fol* Avr1 (SIX4), Avr2 (SIX3) and Avr3 (SIX1) are recognised by tomato immunity receptors, I, I-2
94 and I-3, respectively, leading to effector-triggered immunity (ETI) and disease resistance [5, 22, 23].

95 By understanding the function of *F. oxysporum* effector proteins, and how specific effectors
96 are detected by immunity receptors, we (and others) hope to develop novel disease management

97 strategies targeting vascular wilt diseases. Protein structure studies of effectors provide one avenue
98 to assist this pursuit. Currently, Avr2 represents the only SIX effector whose protein structure has been
99 determined [24]. Interestingly, the β-sandwich fold of Avr2 revealed that this effector shares structural
100 homology to ToxA from *Pyrenophora tritici-repentis* and AvrL567 from *Melampsora lini* [25, 26],
101 despite a lack of sequence identity. The observation of structural classes for effectors without
102 identifiable domains or homologies to proteins of known function has been demonstrated
103 experimentally for four effector structural families, including the so-called MAX (***M**agnaporthe oryzae*
104 **A**vr effectors and To**x**B from *P. tritici-repentis*) [27], RALPH (**R**N**A**se-**L**ike **P**roteins associated with
105 **H**austoria) [28], LARS (***L**eptosphaeria* **A**vi**r**ulence and **S**upressing) [29] and ToxA-like families [24-26].
106 Combining experimental and computational approaches, we present the structural repertoire
107 of sequence unrelated effectors utilised by *Fol* during infection of tomato, including the classification
108 of a new effector family, the FOLD (***Fol* d**ual-domain) effectors. We show using structural comparisons
109 that FOLD effectors are widely distributed in phytopathogenic fungi as well as symbionts. Further, we
110 define the domains and residue that mediate the recognition of the FOLD effector, Avr1, by its
111 corresponding immunity receptor.
112
113 **Results**
114 **The structures of Avr1 and Avr3 adopt a similar dual-domain fold**
115 Avr1 and Avr3 are cysteine-rich effectors that belong to the K2PP (Kex2-processed pro-domain)
116 effector class [30, 31]. To help understand their function, and recognition by I and I-3, we sought to
117 solve their structures using x-ray crystallography. Using our optimised protein production strategy
118 [32], we produced Avr1 (Avr1$^{18-242}$) and Avr3 (Avr3$^{22-284}$) in *Escherichia coli* for crystallisation studies
119 (S1A and S1B Fig). Crystals were obtained for Avr3$^{22-284}$ (after referred to as Avr3) (S1B Fig), however,
120 Avr1$^{18-242}$ failed to crystallise. Previously, we demonstrated that pro-domain removal from the K2PP
121 effector SnTox3 was required to obtain protein crystals [30] and predicted this may also be important
122 for Avr1. Treatment of Avr1$^{18-242}$ with Kex2 *in vitro* resulted in a predominant Avr1 band of ~20 kDa
123 consistent with a mature Avr1$^{59-242}$ protein, however, lower molecular weight bands were also
124 observed suggesting *in vitro* Kex2 cleavage at additional sites [30]. To address this, Avr1 was
125 engineered with an internal thrombin cleavage site (replacing the Kex2 site) to produce a single Avr1^{59-}
126 ^{242} product after thrombin cleavage (after referred to as Avr1). This protein was subsequently used for
127 crystallisation studies resulting in rectangular plate-like crystals (S1A Fig).
128 The crystal structures of Avr1 and Avr3 were solved using a bromide-ion-based single-
129 wavelength anomalous diffraction (SAD) approach (S1 Table), and subsequently were refined using a
130 native dataset to a resolution of 1.65 Å and 1.68 Å, respectively (Fig 1A and 1B). Despite sharing low

amino-acid sequence identity (19.5%), Avr1 and Avr3 adopt a structurally similar dual-domain protein fold. Interpretable, continuous electron density was observed from residue 96 in Avr3 and some regions of the intact pro-domain could be interpreted in the electron density (residues 26-49) (S2A Fig). We also identified regions of the pro-domain (residues 23-45) of Avr1 in the electron density, despite thrombin cleavage of the pro-domain prior to crystallisation (S1A Fig). This indicates that an association between respective Avr and pro-domain was maintained post cleavage *in vitro* (S2B Fig). The importance of this association, if any, remains unclear, but for simplicity, the pro-domains were excluded from further analysis.

The Avr1 and Avr3 N-terminal domain (N-domain), consisting of an N-terminal α-helix followed by five β-strands, and C-terminal domain (C-domain), consisting of a β-sandwich architecture, involving seven or eight β-strands are very similar with a root-mean-square deviation (RMSD) of 2.1 Å and 2.8 Å, respectively (superposition performed using DALI server [33]) (Fig 1). While the individual domains are very similar, superposition of the dual-domain structures returns an RMSD of ~3.4 Å. The larger difference is due to a rotation between the N- and C-domains (Fig 1E). The structures of Avr1 and Avr3, when compared with the solved structures of other fungal effectors, demonstrate that they adopt a unique two-domain fold and represent the founding members of a new structural class of fungal effectors we have designated the FOLD (***Fol* d**ual-domain) effectors.

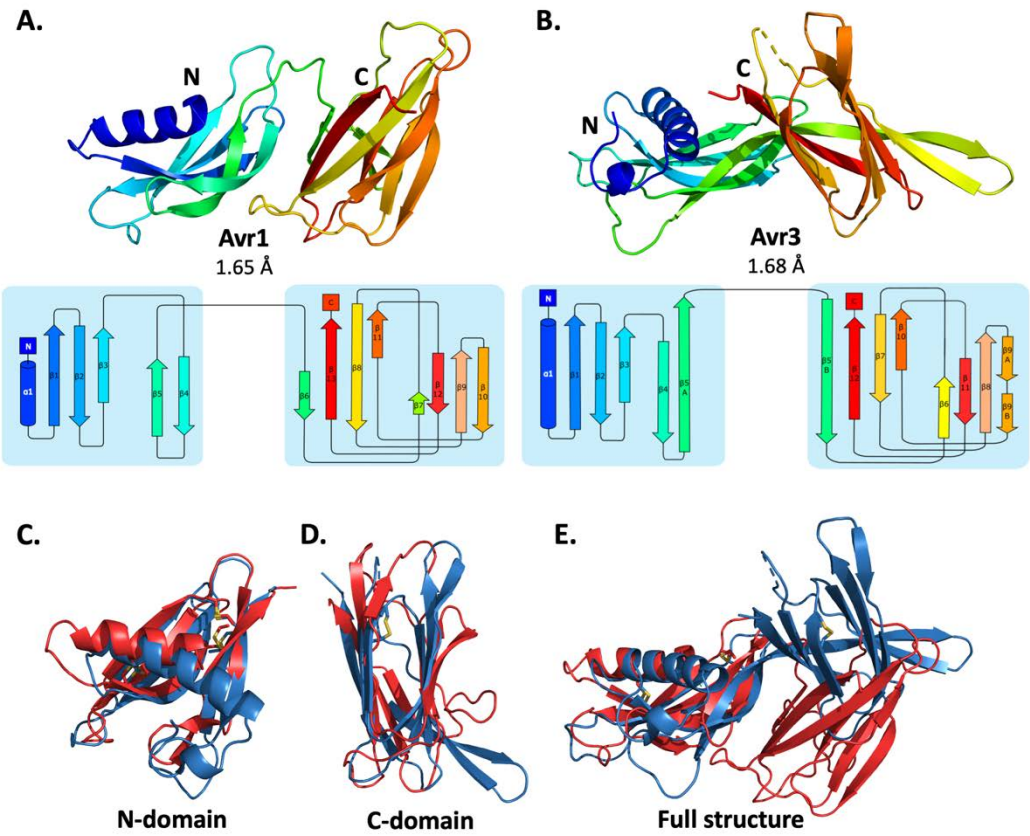

Fig 1. Crystal structures of Avr1 and Avr3 from *Fol* adopt a similar structural fold. Ribbon diagrams of **(A)** Avr1 and **(B)** Avr3 coloured from N- (blue) to C-terminus (red) showing the dual-domain structural fold (top panels), and secondary structure topology map (bottom panels) of Avr1 and Avr3, respectively. For both, the N-domain is shown on the left and the C-domain is shown on the right. The colours of the secondary structural elements match the colours depicted on the crystal structure. Structural alignments of Avr1 (shown in red) and Avr3 (shown in blue) showing **(C)** N-domains alone, **(D)** C-domains alone and **(E)** full structures. Disulfide bonds are shown in yellow. Structural alignment was performed using the pairwise alignment function of the DALI server [33].

157 **SIX6 and SIX13 belong to the FOLD effector family**

158 We were interested to determine if other SIX effectors belonged to the FOLD effector family. One
159 conserved sequence feature observed in Avr1 and Avr3 was the spacing of the six cysteines within the
160 N-domain. We analysed the cysteine spacing of the other SIX effectors and found that SIX6 and SIX13
161 contained a cysteine profile like Avr1 and Avr3 (Fig 2A), suggesting they may be FOLD effectors. With
162 the recent advances in *ab initio* structural prediction by Google DeepMind's AlphaFold2 [34] we
163 predicted the structures of the SIX effectors to determine if, as suggested by our sequence analysis,
164 other SIX effectors are FOLD effector family members.

165 As an initial step we benchmarked the AlphaFold2 predicted models of Avr1 and Avr3
166 (downstream of the Kex2 cleavage site (Avr1$^{59-242}$ and Avr3$^{96-284}$) against our experimentally
167 determined structures (S3 Fig). The AlphaFold2 model of Avr1 returned a low average per-residue
168 confidence score (pLDDT = 55%) and the RMSD was 6.9 Å when model and structure were compared,
169 however, the dual domain architecture was correctly predicted with a Z-score of 11.3 identified using
170 a DALI pair-wise structural comparison (S3A Fig and S3E). The AlphaFold2 model of Avr3 returned a
171 high average pLDDT score (92%) and superimposed well to the solved structure (S3B Fig), despite a
172 slight skew between the orientation of the individual domains (RMSD = 3.6 Å overall; 1.1 Å for the N-
173 domain; 0.8 Å for the C-domain). This demonstrated that accurate FOLD effector prediction was
174 possible using AlphaFold2.

175 We subsequently generated SIX6 and SIX13 models, downstream of the predicted Kex2
176 cleavage site (SIX6$^{58-225}$, SIX13$^{78-293}$), using AlphaFold2 and obtained high average confidence scored
177 models supporting their inclusion in the FOLD family (S4 Fig). To validate this experimentally, we
178 produced SIX6$^{58-225}$ and SIX13$^{22-293}$ (after referred to as SIX6 and SIX13) as described for Avr1/Avr3 and
179 obtained crystals for both proteins (S1 Fig). While the SIX13 crystals diffracted poorly, the SIX6 crystals
180 diffracted x-rays to ~1.9 Å and we solved the structure of SIX6 using the AlphaFold2 generated model
181 as a template for molecular replacement (Fig 2B, S1 Table), confirming its inclusion as a member of
182 the FOLD family. Despite lacking an N-terminal helix, the N-domain contains five β-strands held
183 together by three disulfide bonds with an arrangement, identical to Avr1 and Avr3. The C-domain is
184 an eight stranded β-sandwich that is stabilised by a single disulfide bond (unique to SIX6 compared to
185 Avr1 and Avr3) connecting the β7 and β12 strands. Like Avr1, we identified regions of the pro-domain
186 within the SIX6 structure (residues 29-46), despite cleavage of the pro-domain prior to crystallisation
187 (S2C Fig), but only within one molecule in the asymmetric unit (S2D Fig). For structural analysis, we
188 used the structured region of Chain A of SIX6 (Fig 2B).

189

190 **FOLD effectors are distributed across multiple fungal genera**

191 Despite structural similarities, the FOLD effectors are divergent in their amino acid sequences, sharing
192 15.5 – 22.5% sequence identities between all members (Fig 2A). Homologues of FOLD effectors are
193 dispersed across multiple *formae speciales* of *F. oxysporum* (S5 Fig) [6, 8, 35-38]. We were interested
194 to understand the distribution of FOLD effectors in fungi. Previous structural-based searches
195 performed on effector candidates from *Venturia inaequalis* using Avr1 and Avr3 as templates (which
196 we provided to the authors) found three candidates predicted to be FOLD effectors [39]. Here, we
197 utilised our experimentally determined structures (Avr1, Avr3 and SIX6) to search for other fungal
198 FOLD effectors within the AlphaFold2 protein structure database [40] (https://alphafold.ebi.ac.uk/)
199 using the Foldseek webserver [41]. This analysis identified 124 putative FOLD protein family members
200 across three Divisions of Fungi (Ascomycota, Basidiomycota, and Glomeromycota) (Fig. 2C). Over half
201 of these were found in Ascomycota fungi (73), with expanded families in species of *Fusarium* and
202 *Colletotrichum* (Fig 2C, S2 Table). Expanded families of FOLD proteins were also observed in the
203 division Glomeromycota that form arbuscular mycorrhiza in plant roots, while two putative FOLD
204 effectors were also predicted in the ectomycorrhizal fungus *Piloderma olivaceum* (Division
205 Basidiomycota), which forms mutualistic associations with conifer and hardwood species [41].
206 Structural superposition of members from the three Divisions confirms the structural similarities
207 between the N and C domains and highlights that the major differences identified are the orientation
208 of the domains relative to each other (Fig. 2D), consistent with our experimental data for Avr1, Avr3
209 and SIX6.

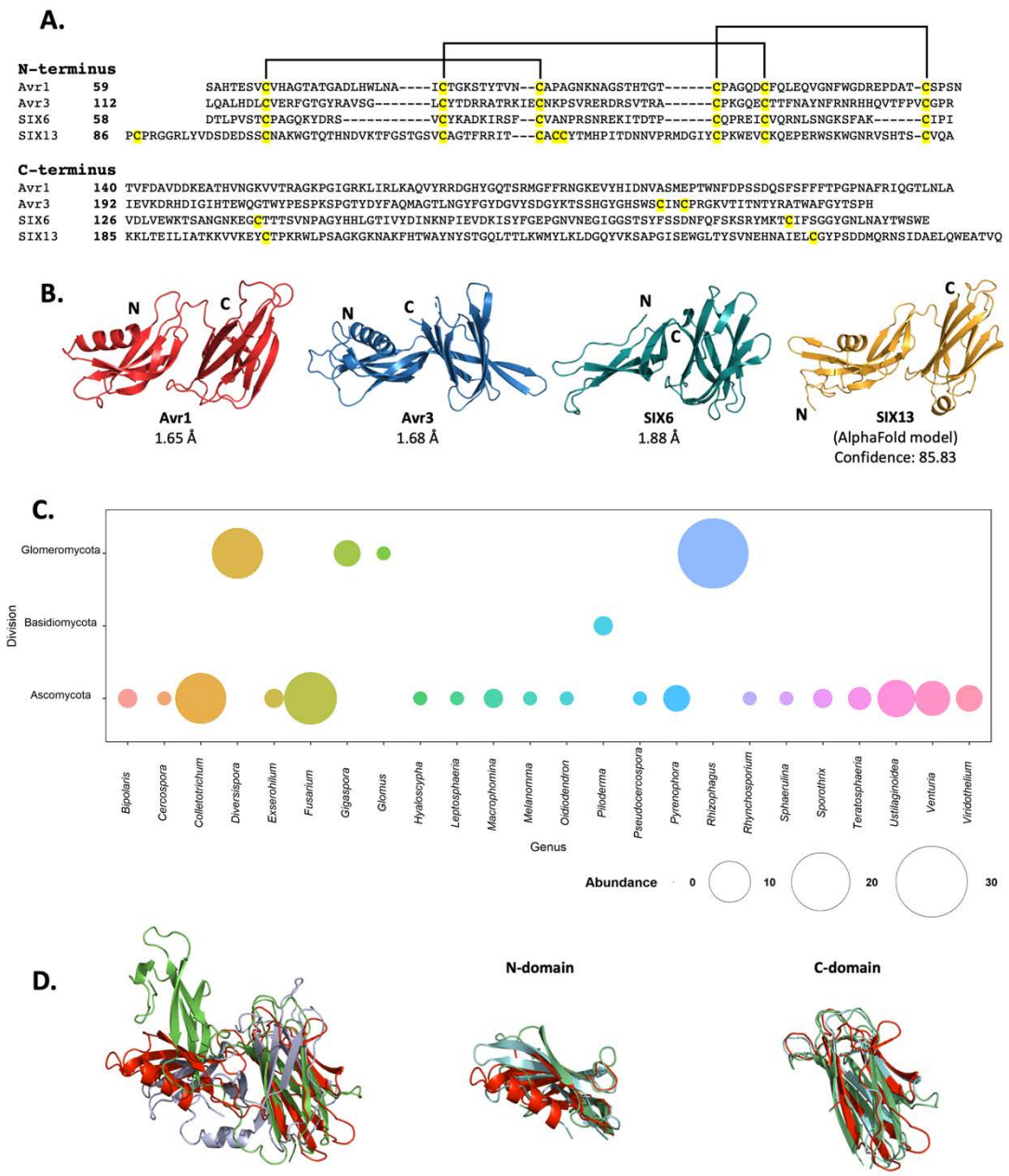

Fig 2. FOLD effector family is distributed within *Fusarium oxysporum* and other fungi. (A) Amino acid sequence alignment of the mature Avr1, Avr3, SIX6 and SIX13 sequences show a common cysteine spacing at the N-terminus. The alignment is split into the N-terminus (N-domain; top panel) and C-terminus (C-domain; bottom panel). Cysteine residues are highlighted in yellow, with common disulfide bonding connectivity, as determined by the crystal structures of Avr1 and Avr3, shown with black lines. **(B)** Ribbon diagrams of the Avr1, Avr3, SIX6 crystal structures and SIX13 AlphaFold2 model show a conserved dual-domain structure. The N- and C-termini are labelled. **(C)** Structure-guided search for putative FOLD effectors across fungi using Foldseek webserver. The size of the circles represent abundance with genus. **(D)** Superposition (structural alignment) of representative putative FOLD effectors from the divisions Glomeromycota and Basidiomycota with Avr1 in ribbon

representation. Putative FOLD protein from *Rhizophagus clarus* (UniProt: A0A2Z6QDJ0) in light blue, and *Piloderma croceum* (UniProt: A0A0C3C2B2) in green. FOLD structural alignment (right), N-domain only (middle), C-domain only (right).

224 **Distinct structural families exist among the other SIX effectors**

225 With the successful utilisation of AlphaFold2 as a model for molecular replacement (SIX6 structure),
226 and structural similarity searches for FOLD effectors, we decided to perform structural comparisons
227 with the remaining SIX effectors. AlphaFold2 modelling of the effectors was conducted on sequences
228 with the signal peptide and putative pro-domain (if present) removed (S6 Fig). The models and
229 experimentally determined SIX effector structures (Avr1, Avr2, Avr3 and SIX6) were compared using
230 the DALI server [33] and a Z-score with a cutoff of >2 was used to indicate structure similarity.

231 The observed structural similarity between the FOLD effectors was high, with Z-scores above
232 8 for all comparisons (Fig 3A). Avr2, a member of the ToxA-like effector family, exhibited structural
233 similarity with the SIX7 and SIX8 models (Z-scores > 5) (Fig 3A). Analysis of the models and topology
234 show that SIX7 and SIX8 both consist of a β-sandwich fold, strongly indicating their inclusion of within
235 the ToxA-like structural family (Fig 3C, S7 Fig).

236 Beyond these described structural families, the Z-scores indicated that two additional, but not
237 yet characterised, structural families exist within the SIX effectors. Here, we define these as structural
238 family 3 and 4, consisting of SIX9 and SIX11, and SIX5 and SIX14, respectively (Fig 3D, E). The models
239 of SIX9 and SIX11 both consist of five β-strands and either two or three α-helices (Fig 3D, S8 Fig),
240 despite sharing only 14% sequence identity. To further our understanding of the putative function of
241 this family we did a structural search against the protein databank (PDB) and found that both
242 structures share structural similarity to various RNA binding proteins (Z-scores > 2.5), such as the RNA
243 recognition motif (RRM) fold of the Musashi-1 RNA-binding domain (PDB code: 5X3Z) [42] with a Z-
244 score of 2.6 and 4.5 for SIX9 and SIX11, respectively.

245 SIX5 and SIX14 also share limited sequence identity (23%) but the structural predictions show
246 a similar secondary-structure topology consisting of two α-helices and four to six β-strands (Fig 3E, S8
247 Fig). We compared the models of SIX5 and SIX14 against the PDB using DALI and identified structural
248 similarity toward the *Ustilago maydis* and *Zymoseptoria tritici* KP6 effector (PDB codes: 4GVB and
249 6QPK) [43], suggesting SIX5 and SIX14 belong to the KP6-like structural family (S7 Fig). Collectively,
250 this analysis demonstrates that 11 of the 14 SIX effectors, group into 4 different structural families.

251

252 **Structural modelling and comparison of an expanded set of *Fol* effectors**

253 The SIX effectors are only a subset of effectors utilised by *Fol* during infection of tomato. Recently, the
254 *Fol* genome was re-sequenced [44] and reannotated in combination with RNAseq data from *Fol*-
255 infected tomato plants [45]. A total of 26 genes encoding novel effector candidates were identified
256 that were consistently upregulated during *Fol* infection [45], which were not previously predicted or
257 predicted incorrectly in the original genome annotation [4]. Of these, 14 genes encoded proteins with

258 no recognised domains or motifs based on their amino acid sequences. We generated structural
259 models using AlphaFold2 of these 14 (S3 Table, S6 Fig) and structurally aligning them using DALI
260 against SIX effector representatives from each family to assess if they fell into any of the established
261 families (Fig 3B). We found the predicted structure of FOXGR_015533 adopts a nine β-stranded
262 sandwich and is likely a member of the ToxA-like class (Fig 3C). PSL1 [17] and FOXGR_015322, here
263 designated PSL2, are sequence related effectors (~85% sequence identity) and show a conserved
264 structure (Fig 3E). Both have Z-scores of >2 against Family 4 and are likely members of this family.
265 Based on this analysis we also suggest an additional structural family. FOXG_18699 and
266 FOXGR_015522 are structurally related (Z-score of 2.2) with a sequence identity of ~29%. While
267 FOXGR_015522 does share some resemblance to Family 4, based on manual alignment (Fig 3F) and
268 domain topology analysis (S8 Fig) these effectors appear to belong to an independent structural
269 family, designated Family 5. Collectively, these data demonstrate that *Fol* utilises multiple structurally
270 related, sequence diverse, effectors during infection of tomato.

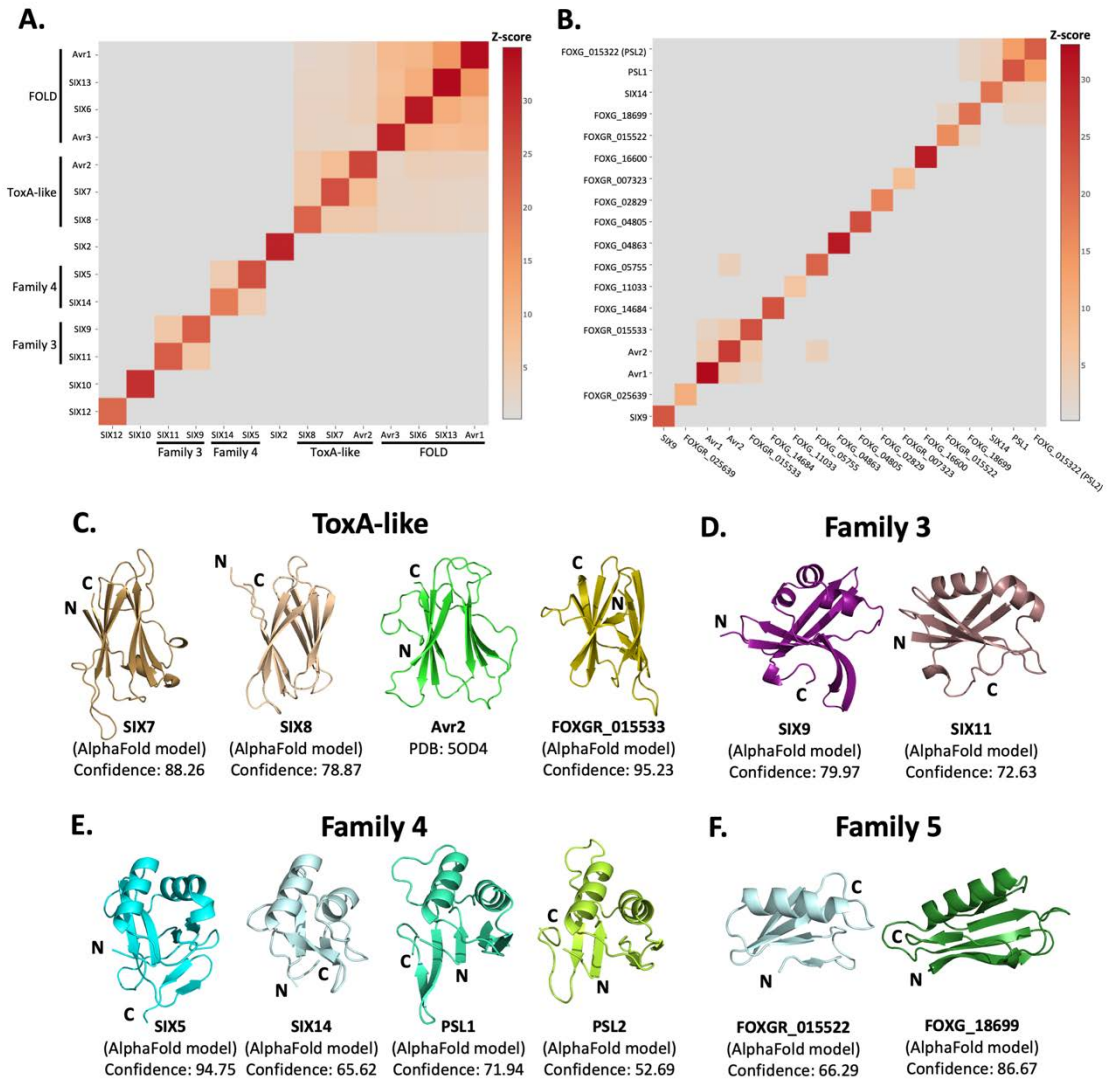

Fig 3. Identification of new putative structural families within the SIX effectors. Heat maps showing the structural similarity of structures and AlphaFold2 models of the **(A)** SIX effectors and **(B)** effector candidates from *Fol* in a structural pairwise alignment. Amino acid boundaries that were modelled for each protein is found in S3 Table. Structural similarity was measured with Z-scores. A cutoff Z-score of 2 was applied for defining structural families. Z-score scale is shown in a grey to red spectrum. **(C)** Cartoon representation of the ToxA-like effectors from *Fol*. AlphaFold2 models of SIX7, SIX8 and FOXGR_015533 effector candidate are putative members of the ToxA-like effector family. The crystal structure of Avr2 [24], another member of the ToxA-like effector family, is shown in green for comparison. Cartoon representations of **(D)** Family 3, **(E)** Family 4 and **(F)** Family 5 consisting of members that are predicted to be structurally similar. The N- and C-termini are labelled. Structural similarity searches were performed using the DALI server [33].

283

284 **Interaction between effector pairs from two structural families**

285 In *Fol, Avr2* and *SIX5*, and *SIX8* and *PSL1* form a similar head-to-head relationship in the genome with
286 shared promoters and are divergently-transcribed (Fig 4A) [16, 17]. Previously, studies concerning
287 Avr2 and SIX5 have demonstrated that the proteins function together and interact directly via yeast-
288 two-hybrid analysis [9]. Homologues of SIX8 and PSL1 from *Focn* (SIX8 and PSE1) are also functionally
289 dependent on each other, however an interaction could not be established in yeast [17]. Here we
290 demonstrate that both protein pairs contain a ToxA-like family member (Avr2, SIX8) and a structural
291 family 4 member (SIX5, PSL1). Considering the predicted structural similarities, we were interested in
292 testing whether *Fol* SIX8 and PSL1 interact.

293 We heterologously produced *Fol* SIX8$^{50-141}$ and PSL1$^{18-111}$ (S1E-F Fig) (after referred to as SIX8
294 and PSL1) and co-incubated the proteins before analysing by size exclusion chromatography (SEC) (Fig
295 4B). The elution profile of PSL1 alone showed a major peak (~12.25 mL) at a volume consistent with a
296 dimeric form of the protein, while SIX8 showed a major peak (~15 mL) consistent with a monomer (Fig
297 4B). Strikingly, when incubated together the major protein peaks migrate to ~12.8 mL. SDS-PAGE
298 analysis confirmed that presence of PSL1 and SIX8, indicating that the migration of both proteins on
299 SEC is altered after incubation (Fig 4B). These data are consistent with PSL1 and SIX8 forming a
300 heterodimer.

301 To understand the structural basis of the interaction, we attempted to solve the structure of
302 the complex, but we were unable to obtain crystals. We subsequently utilised AlphaFold2-Multimer
303 [46] through ColabFold [47], to model the interaction. Manual inspection of the top 5 models (S10A
304 Fig, top model shown Fig. 4C) demonstrated that the thiol side chain of a free cysteine in PSL1 (Cys
305 37) and SIX8 (Cys 58) co-localised in the dimer interface, suggesting that an inter-disulfide bond may
306 mediate the interaction. To test this, we performed intact mass spectrometry of SIX8 and PSL1 (alone
307 and post incubation) under non-reduced and reducing conditions. The mass observed from the
308 incubated SIX8 and PSL1 non-reduced sample contained a predominant species consistent with the
309 combined molecular weight of SIX8 and PSL1 (20777 Da) (Fig 4D, S9G-H Fig). SIX8 and PSL1 failed to
310 form a heterodimer with an unrelated protein containing a free cysteine, suggesting specificity in the
311 interaction (S9I-L Fig). Collectively, these data demonstrated that the SIX8-PSL1 heterodimer is
312 mediated via a disulfide bond.

313 To confirm the involvement of the predicted residues involved, interaction with cysteine
314 mutants of PSL1 and SIX8 (PSL1_C37S$^{18-111}$ and SIX8_C58S$^{50-141}$, after referred to as PSL1_C37S and
315 SIX8_C37S) were analysed (Fig 4E). When PSL1_C37S was incubated with SIX8_C37S or SIX8 alone, the
316 heterodimer was not resolved via SEC (Fig 4D, S10B Fig). This was further confirmed using mass

317 spectrometry (Fig 4C). We crystallised and solved the structure of SIX8_C58S at 1.28 Å (S1E Fig and
318 S10C Fig) which confirms its inclusion within the ToxA-like structural family (S10D Fig).

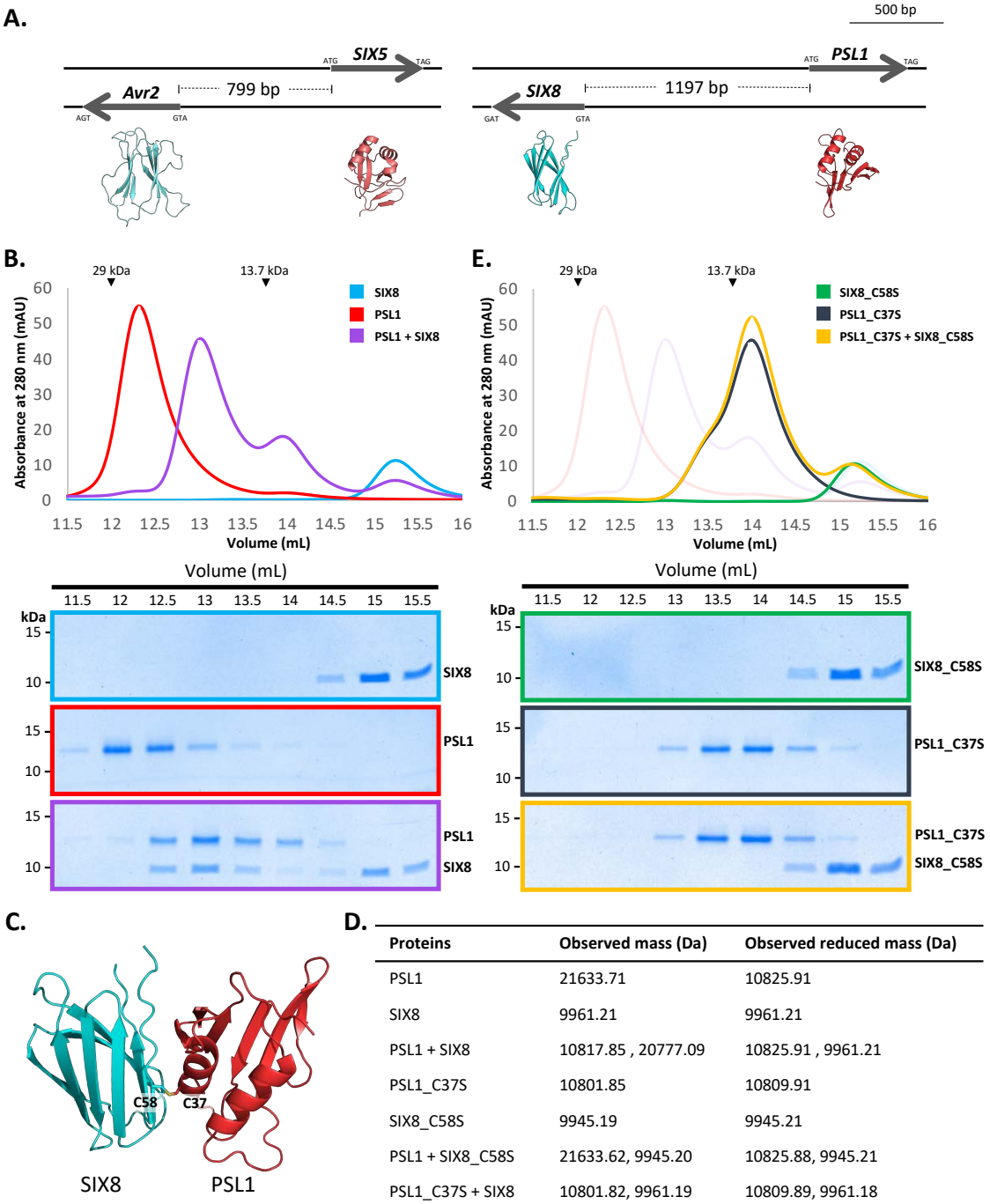

Proteins	Observed mass (Da)	Observed reduced mass (Da)
PSL1	21633.71	10825.91
SIX8	9961.21	9961.21
PSL1 + SIX8	10817.85 , 20777.09	10825.91 , 9961.21
PSL1_C37S	10801.85	10809.91
SIX8_C58S	9945.19	9945.21
PSL1 + SIX8_C58S	21633.62, 9945.20	10825.88, 9945.21
PSL1_C37S + SIX8	10801.82, 9961.19	10809.89, 9961.18

Fig 4. PSL1 and SIX8 interact *in vitro* mediated by an intermolecular disulfide bond. (A) Schematic representation of the *Avr2 (SIX3)* – *SIX5* and *SIX8* – *PSL1* loci within *Fol*. AlphaFold2 models or experimentally solved protein structures are shown underneath. **(B)** Size exclusion chromatograms of PSL1 alone (red), SIX8 alone (blue), PSL1 and SIX8 (purple) (following a 30 min incubation) separated over a Superdex S75 Increase SEC column (top panel). Equal concentrations of the protein were used (note the absorbance of SIX8 at 280 nm is ~0.3 resulting in a smaller absorbance and peak height). Indicated sizes above the chromatogram are based on protein standards run under similar conditions as presented in the manufacturer's column guidelines. Coomassie-stained SDS-PAGE gels depicting

328 samples taken from 500 µL fractions corresponding to the volumes indicated above the gels, with
329 molecular weights (left) and proteins (right) annotated (bottom panels). **(C)** Model of the SIX8-PSL1
330 complex generated by AlphaFold2-Multimer (top model shown). Co-localisation of Cys 58 from SIX8
331 and Cys 37 from PSL1 shown in stick form. **(D)** Observed masses of PSL1 and SIX8 protein mixtures by
332 intact mass spectrometry (MS). Samples were treated with or without the reducing agent DTT prior to
333 MS. The deconvoluted mass spectra of all proteins can be found in S9 Fig. **(E)** As for **(B)** but with
334 PSL1_C37S (black), SIX8_C58S (green), and PSL1_C37S and SIX8_C58S (yellow).

335 **The molecular basis of Avr1 recognition by the I receptor**

336 The structural identification of the FOLD effector family provides an opportunity to understand their
337 recognition by cognate immunity receptors. Here, we focussed on Avr1 (SIX4), which is recognised by
338 the I immunity receptor leading to ETI and disease resistance [19]. Previous studies have shown co-
339 expression of the *I* gene from the M82 tomato cultivar (I^{M82}) with Avr1 in *Nicotiana benthamiana* leads
340 to a cell death response, a proxy for ETI [19]. Conversely, co-expression with the allelic variant
341 ($i^{Moneymaker}$) from the susceptible cultivar Moneymaker does not lead to cell death as the receptor
342 cannot recognise Avr1 [19] (Fig 5B). Here we sought to further define the recognition between Avr1
343 and I utilising the *N. benthamiana* system.

344 To facilitate this, we identified homologues of Avr1 that possess natural residue variation.
345 FonSIX4, a homologue of Avr1 from the watermelon pathogen, *F. oxysporum* f. sp. *niveum* (*Fon*) shares
346 79% identity with Avr1 (Fig 5A). Using the *N. benthamiana* assay we show FonSIX4 is recognised by I
347 receptors from both cultivars (I^{M82} and $i^{Moneymaker}$) (Fig 5B). FonSIX4 and Avr1 differ by 34 residues
348 distributed across both N- and C-domains of the protein (Fig 5A). To narrow down the regions involved
349 in recognition we designed chimeric variants by swapping the N- and C-domains ($Avr1^{N}FonSIX4^{C}$ and
350 $FonSIX4^{N}Avr1^{C}$) (Fig 5A, C). When these were co-expressed with $i^{Moneymaker}$ the cell death response,
351 quantified using ion leakage assays (Fig 5D-E) and visual inspection (S11A Fig), suggest the C-domain
352 of FonSIX4 is recognised by $i^{Moneymaker}$. We separated Avr1 and FonSIX4 proteins into their N- or C-
353 domains and co-expressed with I^{M82} or $i^{Moneymaker}$. Quantification using ion leakage assays demonstrate
354 that the C-domains of Avr1 and FonSIX4 cause cell death when expressed with I^{M82} and $I^{M82/Moneymaker}$,
355 respectively. These data confirm the C-domain is sufficient for I receptor recognition (Fig 5D-E, S12
356 Fig, see S11 Fig for *N. benthamiana* leaf infiltration and protein accumulation data).

357 To understand how Avr1 can escape $i^{Moneymaker}$ recognition, we focussed on surface exposed
358 variant residues (underlined) mapping to four regions within the C-domain (Fig 5A and 5C). Four
359 reciprocal swap mutants between Avr1 and FonSIX4 ($Avr1^{ADVKT}$, $Avr1^{IDH}$, $Avr1^{NGQAR}$, $Avr1^{EEEYGIN}$) were
360 co-expressed with $i^{Moneymaker}$ to identify the residues required for FonSIX4 recognition. $Avr1^{EEEYGIN}$
361 showed consistent ion leakage and cell death similar to FonSIX4 (Fig 5F-G), whereas ion leakage
362 quantification for the other three mutants ($Avr1^{ADVKT}$, $Avr1^{IDH}$, $Avr1^{NGQAR}$) was statistically similar to the
363 non-recognised Avr1 (Fig 5G). The reciprocal mutations in FonSIX4 ($FonSIX4^{KEVYHID}$) significantly
364 reduced ion leakage and cell death response when co-expressed with $i^{Moneymaker}$ compared to FonSIX4
365 (S11D-E Fig, see S11G Fig for protein accumulation data). Collectively, these data show that the C-
366 domain in Avr1 is recognised by I^{M82}, and surface exposed residues in the C-domain allow Avr1 to
367 escape recognition by $i^{Moneymaker}$.

368

369

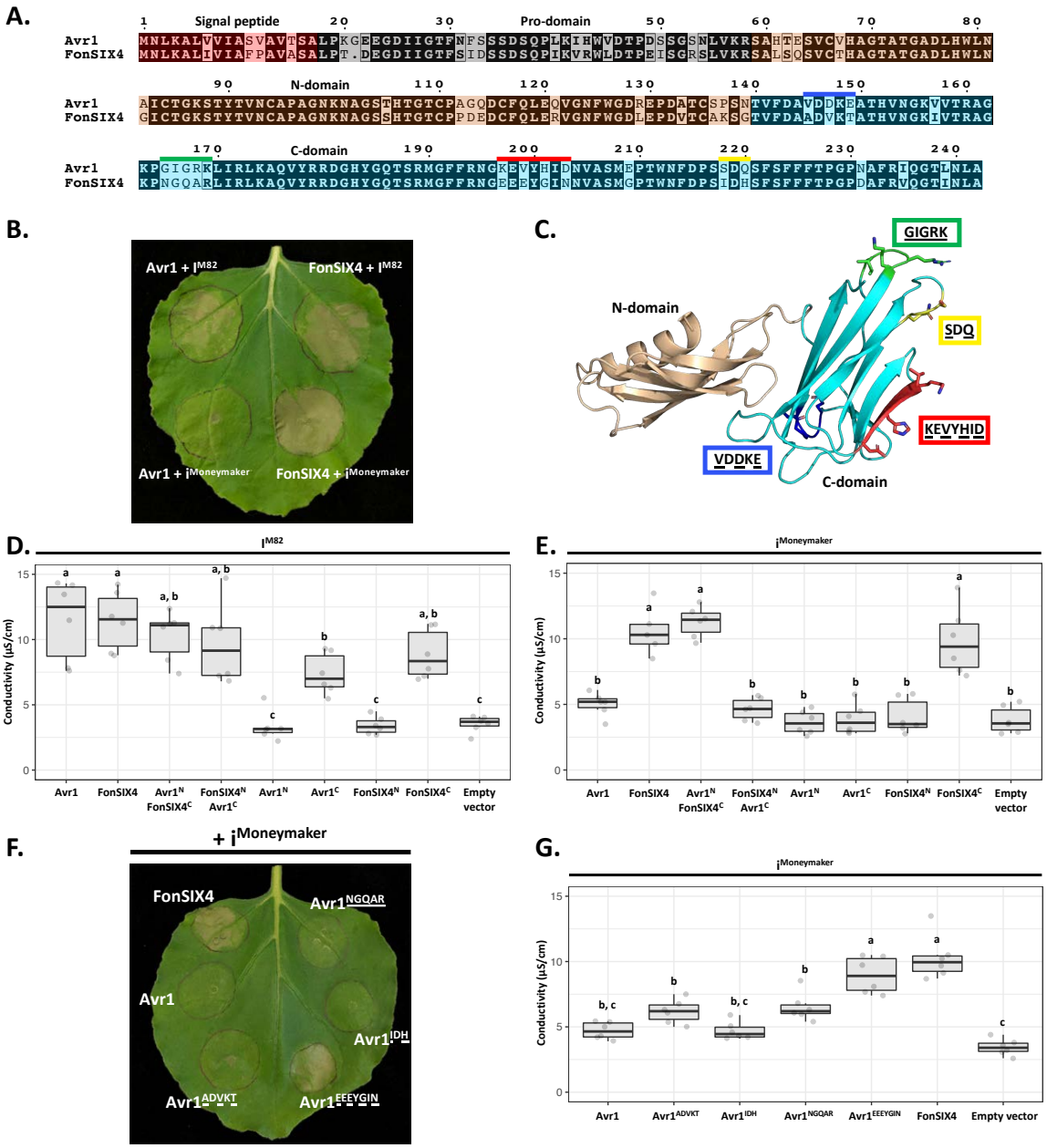

370

371 **Fig 5. The C-domain of Avr1 mediates recognition by the I receptor. (A)** Amino acid sequence
372 alignment of Avr1 and FonSIX4, a homologue from *F. oxysporum* f. sp. *niveum*. The signal peptide, pro-
373 domain, N-domain and C-domain are highlighted in red, grey, beige and blue, respectively. Within the
374 C-domain, surface exposed regions that differ between Avr1 and FonSIX4 are overlined. **(B)** Avr1 and
375 FonSIX4 were transiently expressed in *Nicotiana benthamiana* with either I^{M82} or $i^{Moneymaker}$ via
376 *Agrobacterium*-mediated transformation (n = 6). **(C)** The crystal structure of Avr1, showing the N- and
377 C-domains in beige and light blue, respectively as represented in A. Regions containing variant
378 residues within the C-domain between Avr1 and FonSIX4 are coloured corresponding the overlined
379 colours in A. Variant residues are underlined and represented in stick form. **(D)** Ion leakage

380 conductivity of the Avr1 and FonSIX4 chimeric constructs, and N- and C- domains individually, when
381 transiently co-expressed with I^{M82} or **(E)** $i^{Moneymaker}$. Two additional independent experiments were
382 repeated with similar results (S12 Fig). **(F)** Leaf image and **(G)** ion leakage quantification of the Avr1
383 mutants ($Avr1^{\underline{AD}\underline{V}\underline{KT}}$, $Avr1^{\underline{NGQAR}}$, $Avr1^{\underline{IDH}}$, $Avr1^{\underline{EFE}\underline{Y}\underline{GIN}}$) when transiently co-expressed with $i^{Moneymaker}$ (n =
384 6). Variant residues between Avr1 and FonSIX4 are underlined. Six biological replicates for each
385 construct were measured using an ion leakage assay. One-way ANOVA and post *hoc* Tukey's honestly
386 significant difference tests were performed. Treatments that do not share a letter are significantly
387 different from each other at $p < 0.05$. Leaves were imaged 5 days post infiltration (dpi).

388 **Discussion**

389 Pathogenic fungi are in a continuous arms race with their plant hosts. To aid virulence, but avoid
390 detection, effectors evolve rapidly causing significant diversity at the amino acid sequence level [48].
391 An emerging theme in fungal effector biology is the classification of effectors into families based on
392 structural similarity [49]. Here, we demonstrate that despite their sequence diversity, the *Fol* SIX
393 effectors can be classified into a reduced set of structural families. This observation has implications
394 for functional studies of SIX effectors, and ultimately our understanding of the infection strategies
395 used by *F. oxysporum*.

396

397 **Expanding the structural classes in fungal effectors**

398 To date, five fungal effector families have been defined based on experimentally-determined
399 structural homology, including the MAX [27], RALPH [28, 50, 51], ToxA-like [24-26], LARS [29, 52] and
400 FOLD effectors, defined here. Effectors that fall within many of these structural families are shared
401 across distantly related fungal species. The ToxA-like family includes effectors from fungi that group
402 to both divisions of higher-fungi (Basidiomycota and Ascomycota fungi) [24-26]. The MAX effector
403 family were originally defined as AVR effectors from *M. oryzae* and ToxB from *P. tritici-repentis* [27]
404 but pattern-based sequence searches suggest they are widely distributed amongst the
405 Dothideomycetes and Sordariomycetes [27, 53]. Similarly, LARS effectors, defined in *Leptosphaeria*
406 *maculans* and *Fulvia fulva,* have structural homologues predicted in at least 13 different fungal species
407 [29]. Based on sequence homologues alone, FOLD effectors are well dispersed in fungi with
408 homologues amongst the Sordariomycetes including many *formae speciales* of *F. oxysporum*,
409 *Colletotrichum* and *Ustilaginoidea*. Based on structural comparison of the AlphaFold2 structural
410 database we show that is extended to fungi in three Divisions, including plant pathogens and
411 symbionts. This was supported by a recent study modelling the secretomes of arbuscular mycorrhizal
412 fungi which found enlarged and diversified gene families encoded proteins predicted to share the
413 FOLD effector structure [54]. The exclusive presence of FOLD effectors in plant-colonising fungi may
414 suggest they facilitate plant colonisation in pathogenic and symbiotic fungi [54].

415

416 **Effector structure prediction**

417 Experimentally determining the structures of fungal effectors is not a trivial undertaking. From
418 challenges associated with effector protein production through to hurdles related to structure
419 solution (such as experimental phasing), the research time required to determine an effector structure
420 experimentally ranges from months to many years (sometimes never). Not surprisingly, any reliable
421 structural modelling methods are welcomed by researchers interested in effector biology. To this end,

422 several recent studies have used effector structure prediction to expand our understanding of plant-
423 microbe interactions [55, 56].
424 Work by Bauer and colleagues, prior to the release of AlphaFold2, used structural modelling
425 to show that numerous recognised Avr effectors from the barley powdery mildew-causing fungal
426 pathogen *Blumeria graminis* (*Bgh*) are members of the RALPH effectors class [55]. Seong and Krasileva
427 used similar structural modelling approaches to predict the folds of ~70% of the *Magnaporthe oryzae*
428 secretome [56]. In doing so, they suggested an expansion in the number of MAX effectors and
429 identified numerous sequence-unrelated groups of structural homologues (putative structural
430 classes) within *M. oryzae*. Making use of AlphaFold2, Yan and colleagues show that structurally
431 conserved effectors, including the MAX effector family, from *M. oryzae* are temporally co-expressed
432 during the infection process [57]. In the largest comparison study to date, Seong and Krasileva carried
433 out a large comparative structural genomics study of fungal effectors utilising AlphaFold2 [58]. Their
434 findings support the hypothesis that the structurally conserved effector families are the result of
435 divergent evolution and support previous finding that the structural landscape of effectors is more
436 limited than what is suggested by sequence-diversification.
437 Here, we were in a unique position to apply and benchmark AlphaFold2 against
438 experimentally determined structures for *Fol* effector prediction. We subsequently used AlphaFold2
439 to demonstrate that, within the repertoire of effectors we tested, up to five sequence-unrelated
440 structural families are secreted during *Fol* infection. There are numerous caveats in relying solely on
441 AlphaFold2 to generate structural models of effectors. The accuracy of models generated by
442 AlphaFold2 can decline in cases with low numbers of homologues (~30 sequences in the multiple
443 sequence alignment) [34]. This may help explain the low confidence prediction for SIX4 (Avr1) (S4A
444 Fig), which is only distributed in a few *ff. spp.* of *F. oxysporum*. This poses a potential issue for
445 predicting the structures of fungal effectors that lack homologues. In our hands, we have had mixed
446 results when comparing several unpublished effector structures experimentally determined in our lab
447 to AlphaFold2 models. In some instances, the models are wrong, for example AvrSr50 [59], however,
448 in these cases the AlphaFold2 predictions reported low confidence scores, an important criterion for
449 assessment of model reliability. Despite this, AlphaFold2 models were critical in solving the structure
450 of SIX6 and SIX8, as templates for molecular replacement. This negated the need to derivatise our
451 crystals, a process that we had struggled with for SIX6 crystals, significantly reducing the time and
452 research effort to determine the experimental structures.
453
454 **Structural classes: A starting point for functional characterisation**

455 Given their lack of sequence identity to proteins of known function or conserved motifs, structural
456 determination of effectors is often pursued to provide functional insight and understanding of
457 residues involved in recognition. The existence of structural families of effectors raises the question
458 of whether links can now be made concerning their function based on structural similarities.
459 Unfortunately, the FOLD effectors share little overall structural similarity with known structures in the
460 PDB outside of the similarity with each other. At a domain level, the N-domain of the FOLD effector
461 Avr1 has some structural similarities with cystatin cysteine protease inhibitors (PDB code: 4N6V, PDB
462 code: 5ZC1) [60, 61], and the C-domain with tumour necrosis factors (PDB code: 6X83) [62] and
463 carbohydrate-binding lectins (PDB code: 2WQ4) [63]. Relatively weak hits were observed for
464 Avr3/Six6.

465 Interestingly, the predicted models for SIX9 and SIX11 within Family 3 have structural
466 homology with RNA-binding proteins (PDB code: 3NS6, PDB code: 5X3Z) [42, 64], unrelated to RALPH
467 effectors. Despite this structural homology, close inspection of these models suggests RNA binding is
468 unlikely, as in both models the putative RNA binding surface is disrupted by a disulfide bond.

469 The putative family 4 effectors (SIX5, SIX14, PSL1 and PSL2) have structural homology with
470 KP6 effectors and heavy metal associated (HMA) domains. Metal binding within HMA domains is
471 facilitated by conserved cysteine residues [65], however, their absence in the family 4 effectors
472 suggests they are unlikely to have this activity.

473 The putative family 5 effectors (FOXGR_015522 and FOXG_18699) have structural homology
474 with different proteins within the PDB. FOXGR_015522 is structurally similar to plant defensins (PDB
475 code: 6MRY, PDB code: 7JN6) [66, 67] and K^+ channel-blocking scorpion toxins (PDB code: 1J5J, PDB
476 code: 2AXK) [68, 69]. FOXG_18699 has structural homology with the C-terminal domain of bacterial
477 arginine repressors (PDB code: 1XXB, PDB code: 3CAG) [70, 71].

478

479 **A structural explanation for functional effector pairs**

480 One interesting outcome of this study is a link between structural families and co-operative
481 interactions between effectors. The ToxA-like effectors, Avr2 and SIX8 are known to form functional
482 effector pairs with SIX5 and PSE1 (PSL1-homolouge), respectively [9, 17]. According to our modelling
483 work, both SIX5 and PSL1 are members of structural family 4. *Avr2* and *SIX5* are adjacent divergently-
484 transcribed genes on *Fol* chromosome 14 and the protein products have been shown to physically
485 interact [9]. Likewise, *SIX8* and *PSL1* are adjacent divergently-transcribed genes in the *Fol* genome and
486 we demonstrate here a physical interaction between the proteins. The AlphaFold2-multimer models
487 of the SIX8 and PSL1 heterodimer, drew our attention to the inter-disulfide bond between SIX8 and
488 PSL1 required for the interaction, which we confirmed experimentally. While these residues are

489 conserved in *Focn* SIX8 and PSE1, the Avr2 structure and SIX5 model lack free cysteine residues,
490 suggesting a different mode of interaction.

491 Interestingly, two other *SIX* genes also form a divergently-transcribed gene pair on *Fol*
492 chromosome 14. *SIX7* (ToxA-like family) and *SIX12* possess start codons 2,319 base-pairs apart and
493 potentially share a common promoter. While SIX12 did not group with any structural families, the
494 AlphaFold2 model had a very low prediction confidence (35.5%). On closer inspection of the sequence,
495 we observed that the cysteine spacing in SIX12 closely resembles other family 4 members (S13 Fig),
496 which suggests that SIX12 may also be a family 4 member. We therefore speculate that SIX7 and SIX12
497 may function together, as described for the Avr2/SIX5 and SIX8/PSL1 pairs.
498

499 **Are experimentally derived effector structures still worth the effort?**

500 The potential of machine-learning structural-prediction programs, such as AlphaFold2, heralds an
501 exciting era, especially for a field that has long suffered from a lack of prediction power based on
502 effector sequences. A question now emerges; when prediction model confidence is high, should we
503 bother solving structures experimentally? The answer to such a question will always depend on what
504 the structure is being used for. Ultimately, structural models, whether experimentally or
505 computationally derived, represent information to base and/or develop a hypothesis to subsequently
506 test. Here we demonstrate the power of structure prediction in combination with experimentation,
507 both for validating models and understanding protein:protein interaction interfaces. One interesting
508 observation we made was that while the AphaFold2-multimer models of the SIX8 and PSL1
509 heterodimer were sufficient to highlight the cysteine residues required for mediating the interaction,
510 the models and interaction interfaces differed significantly (S10A Fig). When the modelling was
511 repeated with the SIX8^{C58S} experimentally derived structure included as a template, the interaction
512 models and heterodimer interface were of higher quality and essentially identical (S10E Fig). This
513 observation can be retrospectively reconciled. The region of SIX8 involved in the interaction with PSL1
514 was modelled incorrectly by AlphaFold2 when compared to the structure (S10D Fig). Collectively,
515 these data highlight that some models are good enough, but others maybe better.
516

517 **Effector structural classes and understanding receptor recognition**

518 Understanding the structural basis of plant immunity receptor-effector interactions represent a key
519 step towards engineering plant immunity receptors with novel specificities. Recent structures of
520 nucleotide-binding domain leucine-rich repeat (NLR) proteins reveal exquisite details of these direct
521 interactions [72-74]. The FOLD effectors, Avr1 and Avr3, are recognised by different classes of
522 immunity receptors; I, an LRR-RP [19] and I-3, a SRLK [21]. While the mode of recognition has not yet

523 been described for Avr3, we demonstrate here that Avr1 is recognised at the C-domain (Fig 5). This is
524 significant because it demonstrates that different immunity receptor classes can recognise structural
525 homologues. It might also help explain the function of Avr1 during *Fol* infection. When Houterman
526 and colleagues identified Avr1, they demonstrated that it could suppress plant immunity conferred by
527 the *I-2* and *I-3* receptors [22]. Considering our structural understanding of these FOLD effectors, it is
528 plausible that Avr1 achieves suppression of I-3-mediated immunity by preventing Avr3 recognition
529 through competitive inhibition. The LARS effectors represent another example of effectors that can
530 activate and suppress resistance-gene-mediated immunity. AvrLm4-7 can prevent recognition of
531 AvrLm3 and AvrLm9 (all LARS structural homologues [29]), by their cognate Rlm receptors [75, 76].
532 *Rlm4*, *Rlm7* and *Rlm9* all encode for wall-associated kinases [77, 78], but the identify of *Rlm3* remain
533 unknown. These studies demonstrate that members of at least two different structural effector
534 families can suppress immunity triggered by structurally homologous effectors.
535 Collectively, the results presented here will aid future studies to understand the molecular
536 basis of *F. oxysporum* effector function and recognition, and by extension, the design and engineering
537 of immunity receptors with novel recognition specificities to help protect plants against *Fusarium* wilt
538 disease.
539

540 **Materials and methods**

541

542 **Vectors and gene constructs**

543 SIX6, Avr1Thrombin, SIX6-TEV, SIX8Thrombin, SIX8_C58SThrombin, PSL1, PSL1_C37S and SIX13 coding
544 sequences (without their signal peptides as determined by SignalP-5.0) were codon optimised for
545 expression in *E. coli* and synthesised with Golden-Gate compatible overhangs by Integrated DNA
546 Technologies (IDT, Coralville, USA) (S4 Table). The Kex2 cleavage motif of Avr1 and SIX8 were replaced
547 with a thrombin cleavage motif, and TEV protease cleavage motif for SIX6 for pro-domain processing.
548 Avr1 and Avr3 coding sequences were PCR amplified using *Fol* cDNA as a template with primers
549 containing Golden-Gate compatible overhangs. All genes for *E. coli* expression were cloned into a
550 modified, Golden-Gate-compatible, pOPIN expression vector [79]. The final expression constructs
551 contained N-terminal 6xHis-GB1-tags followed by 3C protease recognition sites. The Golden-Gate
552 digestion, ligation reactions and PCR were carried out as described by Iverson, Haddock [80]. Avr1 and
553 FonSIX4 mutant sequences without the signal peptide were synthesised with compatible overhangs
554 by IDT (S4 Table) and cloned into the pSL vector containing the *Nicotiana tabacum* PR1 signal peptide
555 using the In-fusion cloning kit (Takara Bio USA Inc., San Jose, USA) to allow efficient secretion in *N.*
556 *benthamiana* via *Agrobacterium*-mediated expression. For tagged constructs, Avr1 and FonSIX4
557 mutant sequences and 3xHA tag were amplified with PCR and assembled using In-fusion cloning into
558 the pSL vector. All of the primers were synthesised by IDT (S5 Table). All constructs were verified by
559 sequencing.

560

561 **Protein expression and purification**

562 Sequence-verified constructs were co-expressed with CyDisCo in SHuffle T7 Express C3029 (New
563 England Biolabs (NEB), Ipswich, USA) and purified as previously described [32]. For Avr3, the buffers
564 used after fusion tag cleavage were altered slightly to increase protein stability and a second IMAC
565 step was excluded after the cleavage of the N-terminal fusion tag. During the cleavage step, the
566 protein was dialysed into a buffer containing 10 mM MES pH 5.5 and 300 mM NaCl. The size-exclusion
567 chromatography (SEC) HiLoad 16/600 Superdex 75 pg column (Cytiva) was equilibrated with a buffer
568 containing 10 mM MES pH 5.5 and 150 mM NaCl.

569 For biochemical and crystallisation studies, Avr1 and SIX8 with an internal thrombin cleavage
570 site, and SIX6 with an internal TEV protease cleavage site for pro-domain removal were processed
571 with 2 to 4 units of thrombin from bovine plasma (600-2,000 NIH units/mg protein) (Sigma-Aldrich
572 Inc., St. Louis, USA) per mg of protein at 4°C or TEV protease (produced in-house) until fully cleaved.
573 Fully cleaved proteins were purified further by SEC using a HiLoad 16/600 or HiLoad 26/600 Superdex

574 75 pg column (Cytiva) equilibrated with a buffer containing 10 mM HEPES pH 7.5 or 8.0 and 150 mM
575 NaCl. Proteins were concentrated using a 10 or 3 kDa molecular weight cut-off Amicon centrifugal
576 concentrator (MilliporeSigma, Burlington, USA), snap-frozen in liquid nitrogen and stored at -80°C for
577 future use.
578
579 **Intact mass spectrometry**
580 Proteins were adjusted to a final concentration of 6 µM in 0.1% (v/v) formic acid (FA) for HPLC-MS
581 analysis for untreated samples. For reduced samples, DTT was added to the protein to a final
582 concentration of 10 mM. Proteins were incubated at 60°C for 30 minutes and adjusted to 6 µM in 0.1%
583 (v/v) FA. Intact mass spectrometry on all proteins was carried out as described previously [32]. Data
584 were analysed using the Free Style v.1.4 (Thermo Fisher Scientific) protein reconstruct tool across a
585 mass range of m/z 500 – 2000 and compared against the theoretical (sequence based) monoisotopic
586 mass.
587
588 **Circular dichroism (CD) spectroscopy**
589 The CD spectra of purified effectors of interest were recorded on a Chirascan spectrometer (Applied
590 Photophysics Ltd., UK) at 20°C. Samples were diluted to 10 µM in a 20 mM sodium phosphate buffer
591 at pH 8.0. Measurements were taken at 1 nm wavelength increments from 190 nm to 260 nm. A cell
592 with a pathlength of 1 mm, a bandwidth of 0.5 nm and response time of 4 s were used, with 3
593 accumulations. The data were averaged and corrected for buffer baseline contribution, and visualised
594 using the webserver CAPITO tool with data smoothing [81]. CD analysis was performed on all purified
595 proteins (S14 Fig).
596
597 **Crystallisation, diffraction data collection and crystal structure determination**
598 Initial crystallisation screening was performed for Avr3$^{22-284}$, Avr1$^{18-242}$, Avr1$^{59-242}$, SIX8$^{50-141}$, PSL1$^{18-111}$,
599 SIX6$^{17-225}$, SIX6$^{58-225}$, SIX8_C58S$^{19-141}$, SIX8_C58S$^{50-141}$, PSL1_C37S$^{18-111}$, SIX8-PSL1 complex and SIX13^{22-}
600 ^{293} with and without Kex2 protease using 150 nL protein solution and 150 nL reservoir solution sitting-
601 drop plates at 18°C with commercially available sparse matrix screens.
602 No crystals were obtained for Avr1$^{18-242}$, SIX6$^{17-225}$, SIX8$^{50-141}$, PSL1$^{18-111}$, SIX8-PSL1 complex and
603 SIX13$^{22-293}$. Final crystallisation conditions were optimised for Avr3$^{22-284}$ (0.2 M ammonium sulfate, 0.1
604 M Bis-Tris pH 6.5, 25% (w/v) PEG 3350), Avr1$^{59-242}$ (0.2 M ammonium sulfate, 0.1 M sodium acetate
605 pH 4.5, 17.5% (w/v) PEG 4000), SIX6$^{58-225}$ (0.2 M ammonium tartrate and 20% (w/v) PEG 3350),
606 SIX8_C58S$^{50-141}$ (0.17 M ammonium sulfate, 15% (v/v) glycerol and 25.5% (w/v) PEG 4000), SIX13 (0.2
607 M lithium sulfate, 0.1 M Bis-Tris pH 6.5, 25% (w/v) PEG 3350) and PSL1_C37S$^{18-111}$ (70% (v/v) MPD and

608 0.1 M HEPES pH 7.5). Detailed crystallisation optimisation can be found in the supplementary
609 methods.
610 Crystals were transferred into a cryoprotectant solution containing reservoir solution and 15%
611 (v/v) ethylene glycol, 20% (v/v) glycerol or 10% (v/v) ethylene glycol and 10% (v/v) glycerol. No
612 cryoprotecting was required for SIX8_C58S$^{50-141}$ and PSL1_C37S$^{18-111}$ crystals as the conditions
613 contained sufficient cryoprotectant (glycerol and MPD, respectively) within the crystallisation
614 condition. For experimental phasing, Avr3$^{22-284}$ and Avr1$^{59-242}$ crystals were soaked in a cryoprotectant
615 solution containing 0.5 M or 1 M sodium bromide and vitrified in liquid nitrogen. The datasets for
616 bromide-soaked crystals were collected on the MX1 beamline at the Australian Synchrotron [82] (S1
617 Table). The datasets were processed in XDS [83] and scaled with Aimless in the CCP4 suite [84, 85].
618 The CRANK2 pipeline in CCP4 was used for bromide-based SAD phasing [86, 87]. Models were refined
619 using phenix.refine in the PHENIX package [88] and model building between refinement rounds was
620 done in COOT [89]. The models were used as a template for molecular replacement against high
621 resolution native datasets collected on the MX2 beamline at the Australian Synchrotron [90].
622 Automatic model building was done using AutoBuild [91], and subsequent models were refined with
623 phenix.refine and COOT. For SIX6$^{58-225}$ and SIX8_C58S$^{50-141}$, high confidence *ab initio* models were
624 generated with AlphaFold2 (S3 Fig), which was used as a template for molecular replacement against
625 a native dataset collected on the MX2 beamline at the Australian Synchrotron. The resultant structure
626 was refined as described above.
627
628 **Structural modelling and structural alignment**
629 Structural models were generated with Google DeepMind's AlphaFold2 using the amino acid
630 sequences of SIX effectors and candidates without the signal peptide, as predicted by SignalP-5.0 [92]
631 and predicted pro-domain by searching for a Kex2 cleavage motif (KR, RR or LxxR) if present [30] (S3
632 Table; S6 Fig). For AlphaFold2 predictions the full databases were used for multiple sequence
633 alignment (MSA) construction. All templates downloaded on July 20, 2021 were allowed for structural
634 modelling. For each of the proteins, we produced five models and selected the best model
635 (ranked_0.pdb). Pairwise alignments of the structural models generated by AlphaFold2 and the
636 experimentally determined structures of Avr1 (PDB code: 7T6A), Avr3 (PDB code: 7T69), SIX6 (PDB
637 code: 8EBB) and SIX8 (PDB code: 8EB9) were generated using the DALI server all against all function
638 [33]. Structural similarity between the pairwise alignments were measured using Z-scores from the
639 DALI server.
640
641 **Distribution of FOLD family members across fungi**

642 Structure based searches to determine the distribution of FOLD effectors across other
643 phytopathogens was carried out by searching the experimentally determined Avr1, Avr3 and SIX6
644 structures against available structure databases (Uniprot50, Proteome, Swiss-Prot) using the Foldseek
645 webserver [41] using a 3Di search limited to fungi. An e-value cut off of 0.01 was used, and non-plant
646 associated fungi were removed as well as duplicated results for final analysis. Proteins below 100
647 amino acids, and above 500 amino acids were filtered out and remaining structural hits were manually
648 inspected for similarity to FOLD effectors.
649
650 **Interaction studies between PSL1 and SIX8**
651 To investigate the PSL1 and SIX8 interaction *in vitro*, ~140 µg of PSL1$^{18-111}$ and SIX8$^{50-141}$ individually,
652 and ~140 µg PSL1$^{18-111}$ and 140 µg of SIX8$^{50-141}$ together were injected onto a Superdex 75 Increase
653 10/300 (Cytiva) column pre-equilibrated in 20 mM HEPES pH 7.5, 150 mM NaCl, after a 30 min room
654 temperature incubation. To investigate the residues responsible for the interaction, SIX8_C58S$^{50-141}$
655 and PSL1_C37S$^{18-111}$ mutants were used instead. Samples across the peaks were then analysed by
656 Coomassie-stained SDS-PAGE. To investigate the mode of interaction, PSL1 and SIX8 proteins and
657 mutants at 10 µM were incubated individually or together for 1 hour at room temperature. An
658 unrelated protein with a free cysteine (AvrSr50^{RKQQC}) [59] was used to assess the specificity of the
659 PSL1-SIX8 interaction. Proteins were analysed by intact mass spectrometry with or without the
660 addition of DTT as described above.
661
662 ***Agrobacterium*-mediated gene expression in *N. benthamiana***
663 *Agrobacterium tumefaciens* cultures containing the pSL constructs and pSOUP [93] were diluted to an
664 OD_{600} of 1.0 in 10 mM MES pH 5.5 buffer containing 10 mM $MgCl_2$ and 200 µM acetosyringone and
665 incubated in the dark for 2 hours. For co-infiltrations, cultures were mixed together in equal volumes.
666 Resuspensions were infiltrated into 4 – 5-week-old *N. benthamiana* leaves. Infiltrated plants were kept
667 in a 25°C controlled temperature room with a 16-hour photoperiod. Leaves were imaged 4 – 7 dpi.
668
669 **Ion leakage assay**
670 Six biological replicates each consisting of three leaf discs (7 mm diameter) were harvested from
671 leaves infiltrated with *Agrobacterium* 20 - 24 hours post infiltration and incubated in 7 mL of water in
672 a 6-well culture plate. The water was replaced after 40 - 60 min. The leaf discs were incubated in water
673 at room temperature and the conductivity was measured after 24 - 48 hours.
674
675 **Immunoblot analysis of proteins expressed in *N. benthamiana***

676 *N. benthamiana* leaves infiltrated with *A. tumefaciens* cultures were harvested 3 dpi. Leaf tissue was
677 frozen in liquid nitrogen, ground into a powder and resuspended in 3x Laemmli buffer containing 0.2
678 mM DTT and 5 M urea to extract proteins. Samples were boiled for 10 min and centrifuged at 13000
679 xg to remove leaf debris. Proteins were separated by SDS-PAGE and transferred by electroblotting
680 onto PVDF membranes. Protein blots were probed with anti-HA antibodies conjugated to horseradish
681 peroxidase (Roche, Switzerland, 12013819001, 1:4000). Immunoblots were visualised with Pierce ECL
682 Plus Western Blotting Substrate (Thermo Fisher Scientific) as described by the manufacturer.
683 Membranes were stained with Ponceau S to assess protein loading.
684

685 **Acknowledgements**

686 This work was supported by the Australian Research Council (ARC DP200100388 D.J./S.W.) and the
687 Australian Academy of Science (Thomas Davies Grant). S.W. was funded by an ARC Future Fellowship
688 (FT200100135) and supported by the ANU Future Scheme (35665). L.M. was funded by an ARC
689 Discovery Early Career Researcher Award (DE170101165). A.S. was a recipient of the AINSE Honours
690 Scholarship Program, and D.Y. and C.M. held an AINSE Postgraduate Research Award. P.K. was
691 supported by a Netaji Subhas ICAR International Fellowship. The authors acknowledge the use of the
692 ANU crystallisation facility. This research was undertaken in part using the MX2 beamline at the
693 Australian Synchrotron, part of ANSTO, and made use of the Australian Cancer Research Foundation
694 (ACRF) detector. The authors acknowledge use of the Australian Synchrotron MX facility and thank
695 the staff for their support. The coordinates and structure factors for Avr1, Avr3, SIX6 and SIX8 have
696 been deposited in the Protein Data Bank with accession number 7T6A, 7T69, 8EBB and 8EB9,
697 respectively.
698

699 **Figure legends**

700 **Fig 1. Crystal structures of Avr1 and Avr3 from *Fol* adopt a similar structural fold.** Ribbon diagrams
701 of **(A)** Avr1 and **(B)** Avr3 coloured from N- (blue) to C-terminus (red) showing the dual-domain
702 structural fold (top panels), and secondary structure topology map (bottom panels) of Avr1 and Avr3,
703 respectively. For both, the N-domain is shown on the left and the C-domain is shown on the right. The
704 colours of the secondary structural elements match the colours depicted on the crystal structure.
705 Structural alignments of Avr1 (shown in red) and Avr3 (shown in blue) showing **(C)** N-domains alone,
706 **(D)** C-domains alone and **(E)** full structures. Disulfide bonds are shown in yellow. Structural alignment
707 was performed using the pairwise alignment function of the DALI server [33].

708

709 **Fig 2. FOLD effector family is distributed within *Fusarium oxysporum* and other fungi. (A)** Amino acid
710 sequence alignment of the mature Avr1, Avr3, SIX6 and SIX13 sequences show a common cysteine
711 spacing at the N-terminus. The alignment is split into the N-terminus (N-domain; top panel) and C-
712 terminus (C-domain; bottom panel). Cysteine residues are highlighted in yellow, with common
713 disulfide bonding connectivity, as determined by the crystal structures of Avr1 and Avr3, shown with
714 black lines. **(B)** Ribbon diagrams of the Avr1, Avr3, SIX6 crystal structures and SIX13 AlphaFold2 model
715 show a conserved dual-domain structure. The N- and C-termini are labelled. **(C)** Structure-guided
716 search for putative FOLD effectors across fungi using Foldseek webserver. The size of the circles
717 represent abundance with genus. **(D)** Superposition (structural alignment) of representative putative
718 FOLD effectors from the divisions Glomeromycota and Basidiomycota with Avr1 in ribbon
719 representation. Putative FOLD protein from *Rhizophagus clarus* (UniProt: A0A2Z6QDJ0) in light blue,
720 and *Piloderma croceum* (UniProt: A0A0C3C2B2) in green. FOLD structural alignment (right), N-domain
721 only (middle), C-domain only (right).

722

723 **Fig 3. Identification of new putative structural families within the SIX effectors.** Heat maps showing
724 the structural similarity of structures and AlphaFold2 models of the **(A)** SIX effectors and **(B)** effector
725 candidates from *Fol* in a structural pairwise alignment. Amino acid boundaries that were modelled for
726 each protein is found in S3 Table. Structural similarity was measured with Z-scores. A cutoff Z-score of
727 2 was applied for defining structural families. Z-score scale is shown in a grey to red spectrum. **(C)**
728 Cartoon representation of the ToxA-like effectors from *Fol*. AlphaFold2 models of SIX7, SIX8 and
729 FOXGR_015533 effector candidate are putative members of the ToxA-like effector family. The crystal
730 structure of Avr2 [24], another member of the ToxA-like effector family, is shown in green for
731 comparison. Cartoon representations of **(D)** Family 3, **(E)** Family 4 and **(F)** Family 5 consisting of

732 members that are predicted to be structurally similar. The N- and C-termini are labelled. Structural
733 similarity searches were performed using the DALI server [33].
734
735 **Fig 4. PSL1 and SIX8 interact *in vitro* mediated by an intermolecular disulfide bond. (A)** Schematic
736 representation of the *Avr2 (SIX3)* – *SIX5* and *SIX8* – *PSL1* loci within *Fol*. AlphaFold2 models or
737 experimentally solved protein structures are shown underneath. **(B)** Size exclusion chromatograms of
738 PSL1 alone (red), SIX8 alone (blue), PSL1 and SIX8 (purple) (following a 30 min incubation) separated
739 over a Superdex S75 Increase SEC column (top panel). Equal concentrations of the protein were used
740 (note the absorbance of SIX8 at 280 nm is ~0.3 resulting in a smaller absorbance and peak height).
741 Indicated sizes above the chromatogram are based on protein standards run under similar conditions
742 as presented in the manufacturer's column guidelines. Coomassie-stained SDS-PAGE gels depicting
743 samples taken from 500 µL fractions corresponding to the volumes indicated above the gels, with
744 molecular weights (left) and proteins (right) annotated (bottom panels). **(C)** Model of the SIX8-PSL1
745 complex generated by AlphaFold2-Multimer (top model shown). Co-localisation of Cys 58 from SIX8
746 and Cys 37 from PSL1 shown in stick form. **(D)** Observed masses of PSL1 and SIX8 protein mixtures by
747 intact mass spectrometry (MS). Samples were treated with or without the reducing agent DTT prior to
748 MS. The deconvoluted mass spectra of all proteins can be found in S9 Fig. **(E)** As for **(B)** but with
749 PSL1_C37S (black), SIX8_C58S (green), and PSL1_C37S and SIX8_C58S (yellow).
750
751 **Fig 5. The C-domain of Avr1 mediates recognition by the I receptor. (A)** Amino acid sequence
752 alignment of Avr1 and FonSIX4, a homologue from *F. oxysporum* f. sp. *niveum*. The signal peptide, pro-
753 domain, N-domain and C-domain are highlighted in red, grey, beige and blue, respectively. Within the
754 C-domain, surface exposed regions that differ between Avr1 and FonSIX4 are overlined. **(B)** Avr1 and
755 FonSIX4 were transiently expressed in *Nicotiana benthamiana* with either I^{M82} or $i^{Moneymaker}$ via
756 *Agrobacterium*-mediated transformation (n = 6). **(C)** The crystal structure of Avr1, showing the N- and
757 C-domains in beige and light blue, respectively as represented in A. Regions containing variant
758 residues within the C-domain between Avr1 and FonSIX4 are coloured corresponding the overlined
759 colours in A. Variant residues are underlined and represented in stick form. **(D)** Ion leakage
760 conductivity of the Avr1 and FonSIX4 chimeric constructs, and N- and C- domains individually, when
761 transiently co-expressed with I^{M82} or **(E)** $i^{Moneymaker}$. Two additional independent experiments were
762 repeated with similar results (S12 Fig). **(F)** Leaf image and **(G)** ion leakage quantification of the Avr1
763 mutants ($Avr1^{\underline{AD}\underline{V}\underline{KT}}$, $Avr1^{\underline{NGQAR}}$, $Avr1^{\underline{IDH}}$, $Avr1^{\underline{E}\underline{EE}\underline{Y}\underline{GIN}}$) when transiently co-expressed with $i^{Moneymaker}$ (n =
764 6). Variant residues between Avr1 and FonSIX4 are underlined. Six biological replicates for each
765 construct were measured using an ion leakage assay. One-way ANOVA and post *hoc* Tukey's honestly

766 significant difference tests were performed. Treatments that do not share a letter are significantly
767 different from each other at $p < 0.05$. Leaves were imaged 5 days post infiltration (dpi).

768 **Supplementary Figures**

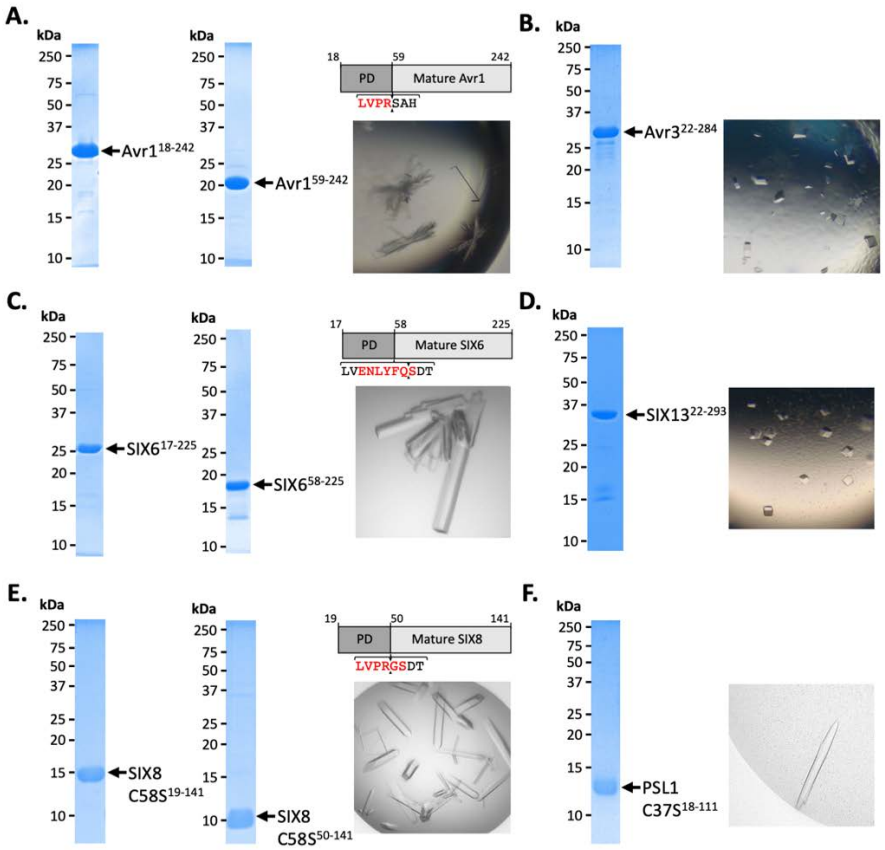

769

770 **S1 Fig. Crystallisation of Avr1, Avr3, SIX6, SIX8, SIX13 and PSL1. (A)** Coomassie-stained gel showing
771 Avr1$^{18-242}$ (left panel) and mature Avr1$^{59-242}$ cleaved *in vitro* with thrombin (middle panel). Schematic
772 of Avr1 engineered with an internal thrombin cleavage site replacing the Kex2 cleavage motif after
773 the pro-domain (PD) (top right panel). Optimised crystals of Avr1$^{59-242}$ (bottom right panel) **(B)**
774 Coomassie-stained gel showing purified Avr3$^{22-284}$ used for crystallisation studies (left panel).
775 Optimised crystals of Avr3 (right panel). **(C)** Coomassie-stained gel showing SIX6$^{17-225}$ (left panel) and
776 mature SIX6$^{58-225}$ cleaved *in vitro* with TEV protease (middle panel). Schematic of SIX6 engineered with
777 an internal TEV protease cleavage site replacing the Kex2 cleavage motif after the PD (top right panel).
778 Optimised crystals of SIX6$^{58-225}$ (bottom right panel). **(D)** Coomassie-stained gel showing SIX13$^{22-293}$
779 protein (left panel). Optimised crystals of SIX13 (right panel). Kex2 protease was added to the protein
780 at a 1:200 protease to protein ratio prior to crystal tray setup. **(E)** Coomassie-stained gel showing
781 SIX8_C58S$^{19-141}$ (left panel) and mature SIX8_C58S$^{50-141}$ cleaved *in vitro* with thrombin (middle panel).
782 Schematic of SIX8 engineered with an internal thrombin cleavage site replacing the Kex2 cleavage
783 motif (top right panel). Optimised crystals of SIX8_C58S$^{50-141}$ (bottom right panel). **(F)** Coomassie-

784 stained gel showing PSL1_C37S$^{18-111}$ protein (left panel). Optimised crystals of PSL1_C37S$^{18-111}$ (right
785 panel).

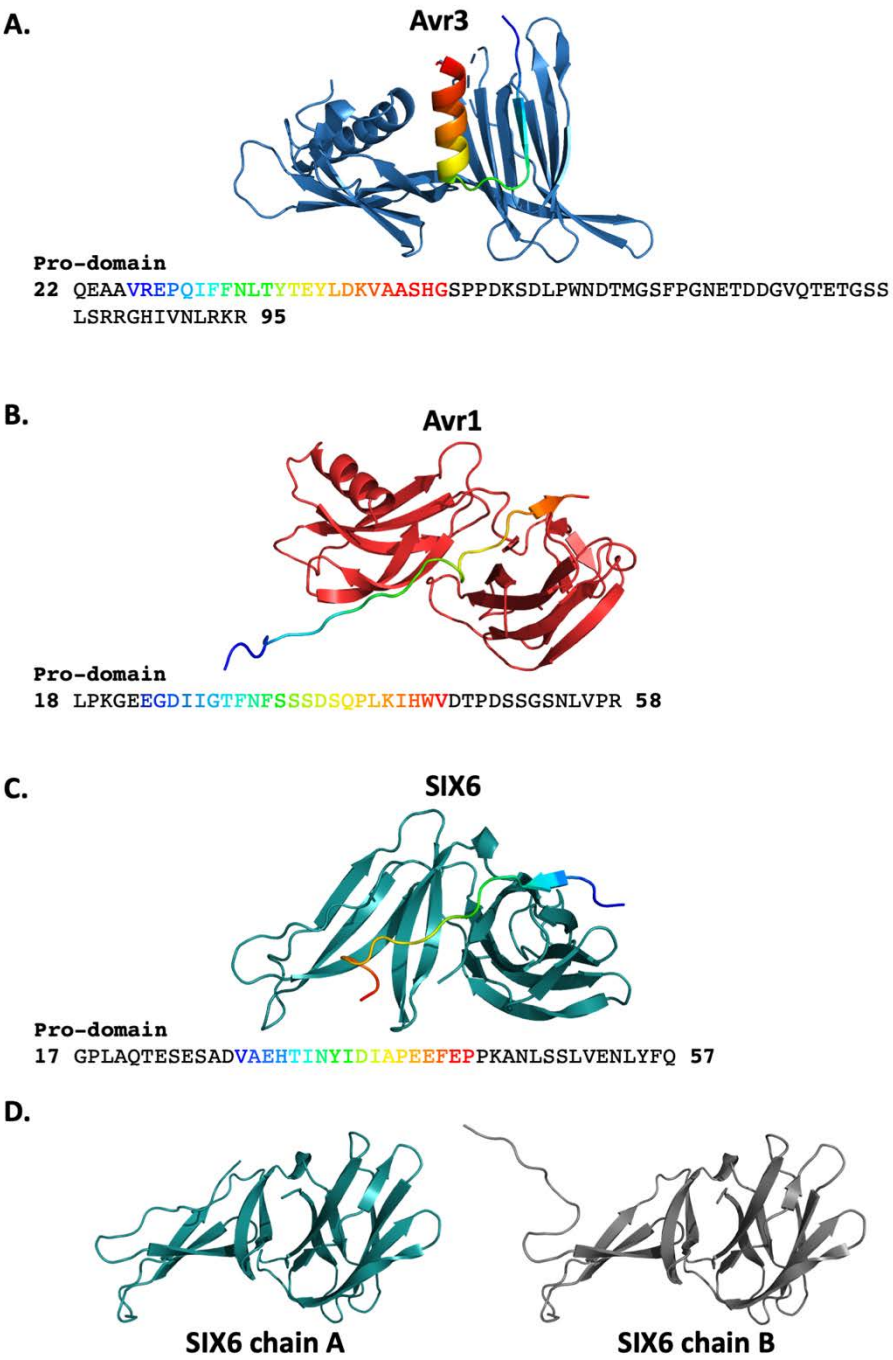

S2 Fig. Continuous electron density of the pro-domain is present in the crystal structures of Avr1, Avr3 and SIX6. The crystal structure of **(A)** Avr3, **(B)** Avr1 and **(C)** SIX6 with the pro-domain shown in rainbow (top panels). The amino acid sequence of the pro-domain of Avr3, Avr1 and SIX6 with residues observed in the electron density shown in rainbow text (bottom panels). Residues with no density observed are shown in black. For SIX6, electron density corresponding to the pro-domain was only associated to chain A. **(D)** Different orientations of the N-terminal region of SIX6 between chains A and B. Chain A was used in subsequent structural analysis.

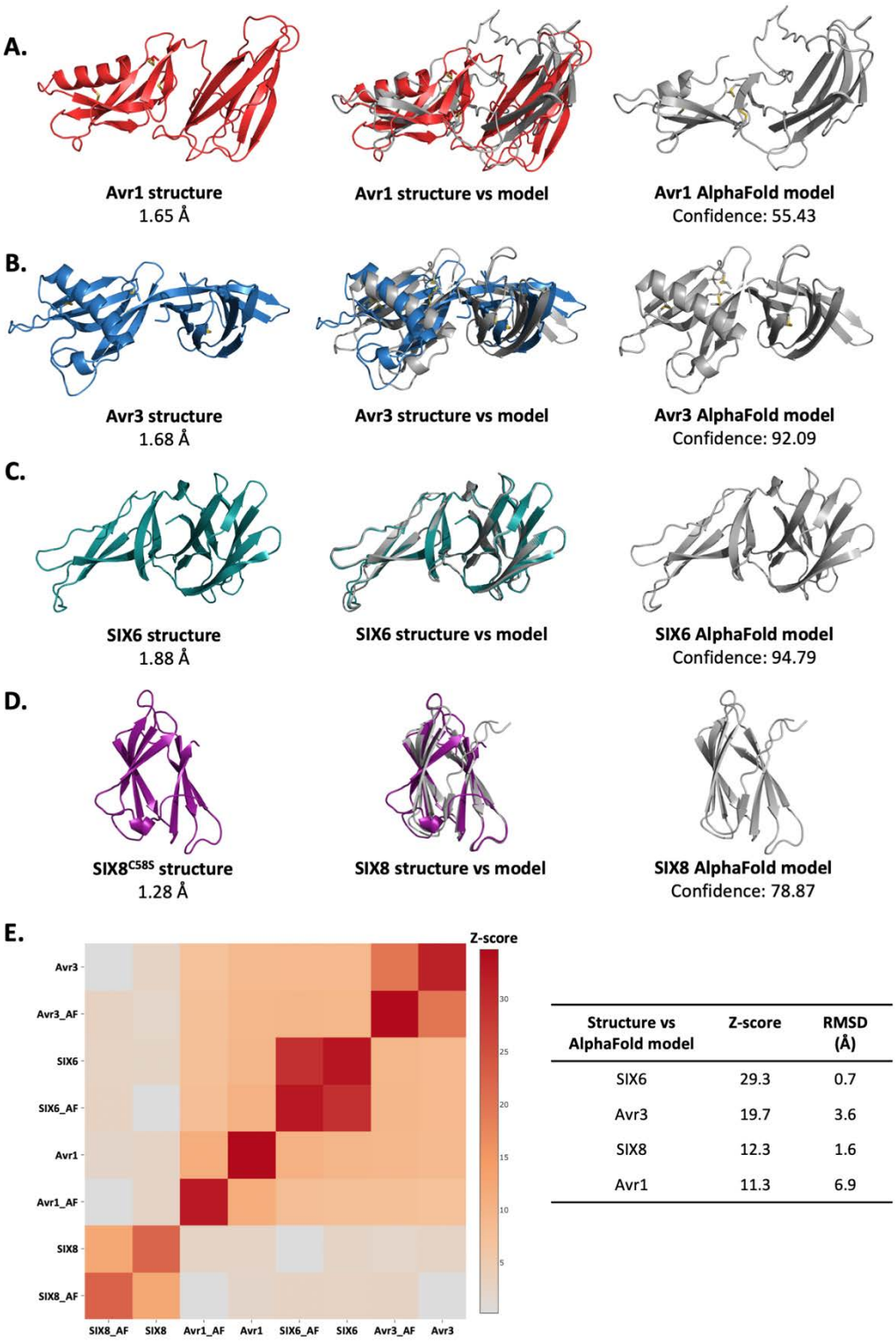

Structure vs AlphaFold model	Z-score	RMSD (Å)
SIX6	29.3	0.7
Avr3	19.7	3.6
SIX8	12.3	1.6
Avr1	11.3	6.9

S3 Fig. Comparison of AlphaFold2 models against the experimentally solved structures of Avr1, Avr3, SIX6 and SIX8. The crystal structures of **(A)** Avr1, **(B)** Avr3, **(C)** SIX6 and **(D)** SIX8 (left panels) and AlphaFold2 models [34] (right panels). Crystal structures and AlphaFold2 models of the full structures (middle panels) were superimposed using the pairwise and all against all functions on the DALI server

[33]. **(E)** Heat map of the structural similarity between crystal structures and AlphaFold2 models (left panel). Z-score and RMSD values are shown in the right panel.

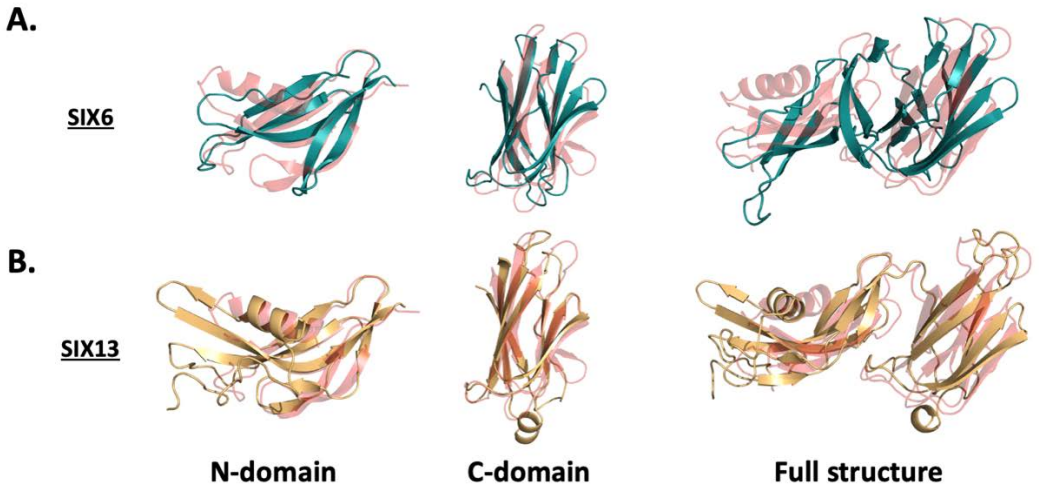

802

803 **S4 Fig. Structural alignments of SIX6 and SIX13 with Avr1. (A)** SIX6 crystal structure and **(B)** SIX13
804 AlphaFold2 model aligned with Avr1 using the N-domains alone (left panel), C-domains alone (middle
805 panel) and full structure (right panel). Structural alignment was performed using the pairwise
806 alignment function on the DALI server [33].

	FOLD effectors			
	Avr1	**Avr3**	**SIX6**	**SIX13**
Fusarium oxysporum f. sp.		*pisi*		
		melonis		
		cubense TR4		
			vasinfectum	
	niveum		*niveum*	
			passiflorae	
		fragariae		*fragariae*
		conglutinans		
				medicaginis
	spinaciae			

807

808 **S5 Fig. Homologues of FOLD effectors are dispersed across multiple *formae speciales* of *F.***
809 ***oxysporum.*** Functional homologues of Avr1 (SIX4), Avr3 (SIX1), SIX6 and SIX13 reported in literature
810 were assessed [6, 8, 35-38].

811

812

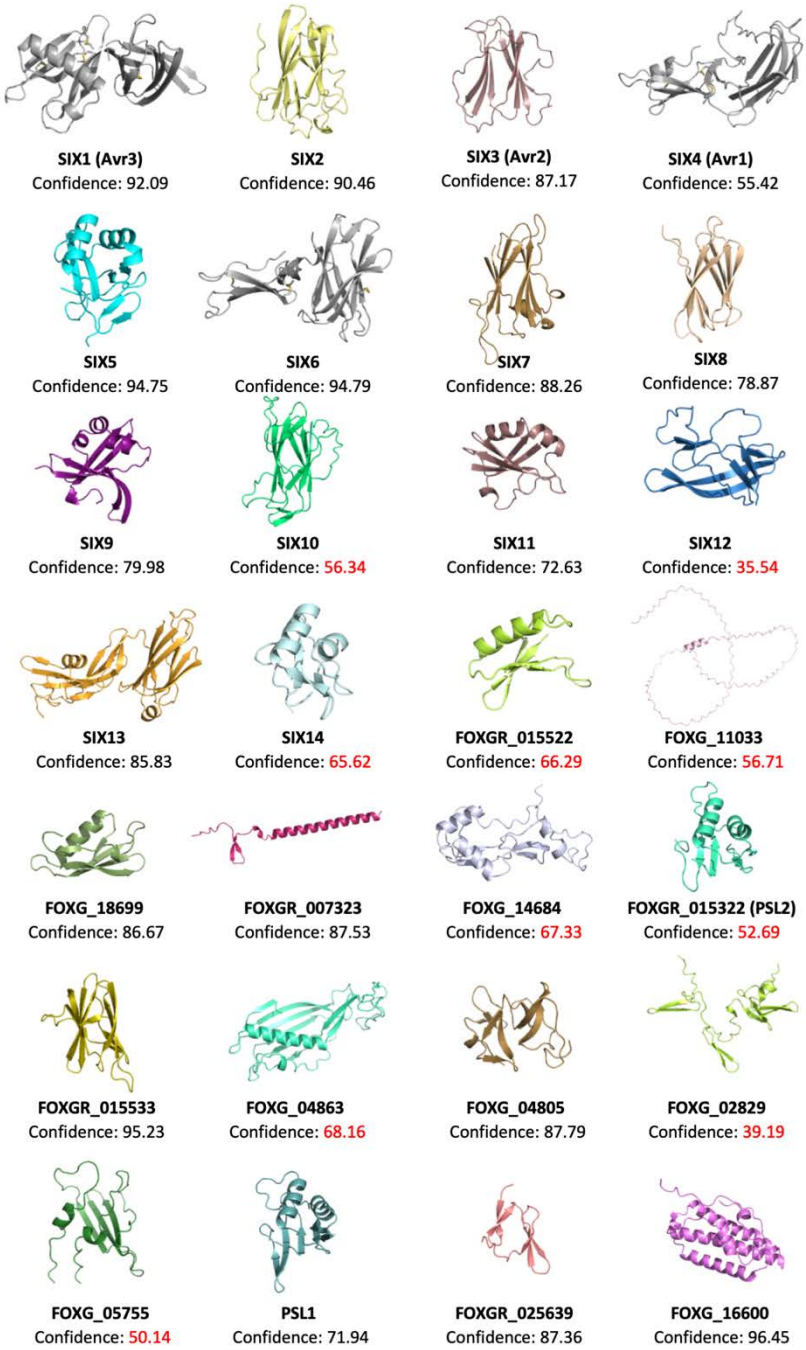

S6 Fig. AlphaFold2 models of all SIX effectors and effector candidates. Signal peptides were identified using SignalP-5.0 [92] and removed prior to amino acid sequences being input into AlphaFold2 [34]. Any putative pro-domains were identified by searching for a Kex2-like protease site [31] and removed. The sequence inputs used can be found in S3 Table.

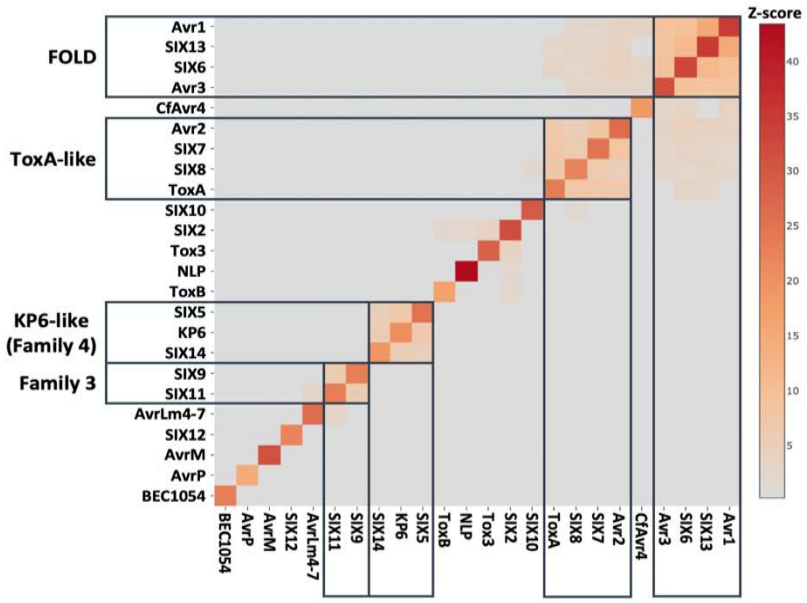

S7 Fig. Structural similarity of SIX effectors against representative solved effector structures from known structural families. The solved structures of Avr1, Avr2, Avr3 and SIX6, and AlphaFold2 models the remaining SIX effectors were compared with the structures of ToxA (ToxA-like), ToxB (MAX), Tox3 (Tox3-like), BEC1054 (RALPH), AvrLm4-7 (LARS), AvrP (Zinc finger), CfAvr4 (CBM14-like), AvrM (WY-like), NLP (Actinoporin-like) and KP6 (KP6-like). Structural alignment was performed using the all against all function on the DALI server [33]. Structural similarity was measured using Z-score. Groupings with Z-scores > 2 were outlined.

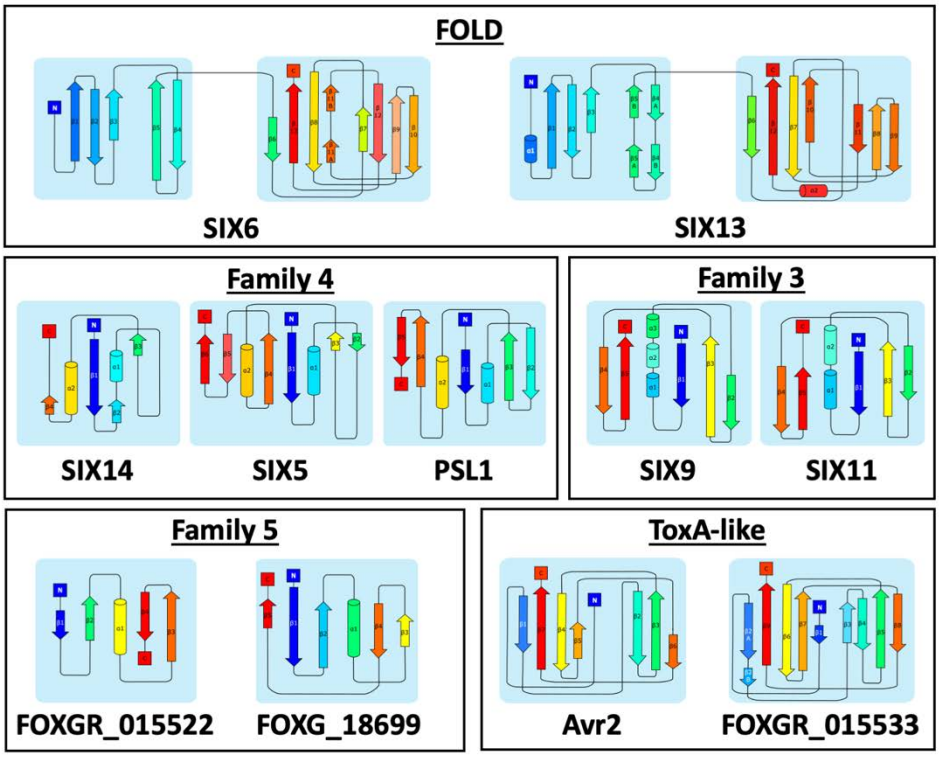

S8 Fig. Secondary structure topology maps of representative SIX structural family members. Secondary topology maps of AlphaFold2 models were generated using Pro-origami [94] and manually edited in Inkscape. The β-strands and α-helices are represented by arrows and cylinders, respectively. The secondary structural elements are coloured in rainbow, from blue at the N-terminus to red at the C-terminus.

A. **PSL1**

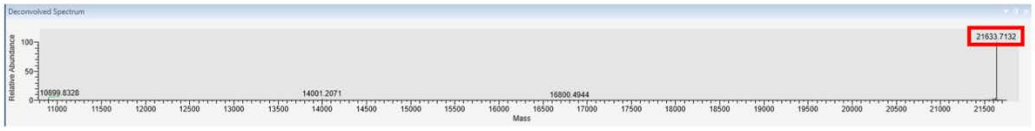

B. **PSL1 reduced**

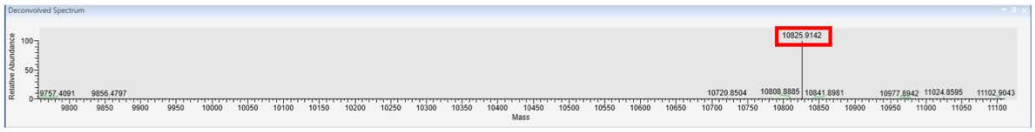

C. **SIX8**

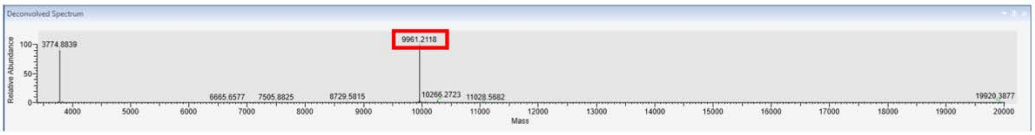

D. **SIX8 reduced**

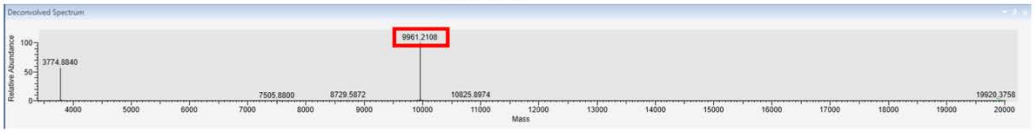

E. **AvrSr50^{RKQQC}**

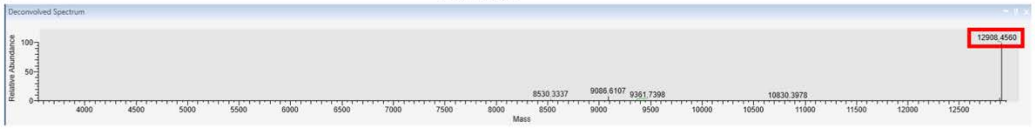

F. **AvrSr50^{RKQQC} reduced**

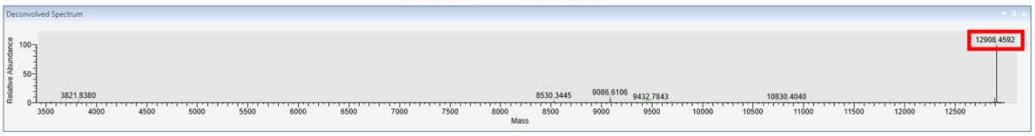

G. **PSL1 + SIX8**

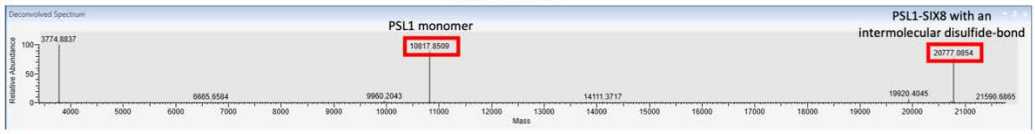

H. **PSL1 + SIX8 reduced**

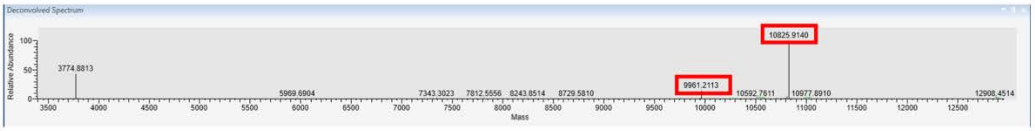

I. **PSL1 + AvrSr50^{RKQQC}**

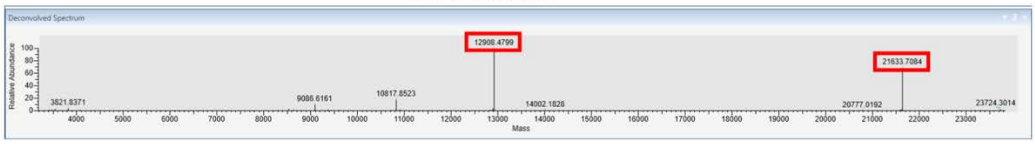

835

J. **PSL1 + AvrSr50^{RKQQC} reduced**

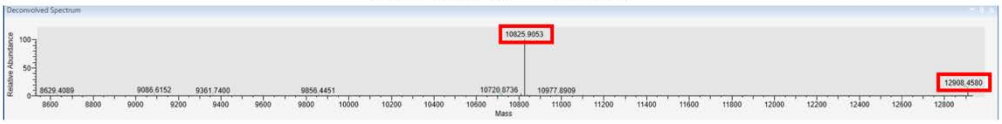

K. **SIX8 + AvrSr50^{RKQQC}**

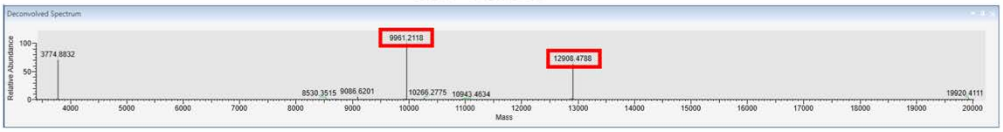

L. **SIX8 + AvrSr50^{RKQQC} reduced**

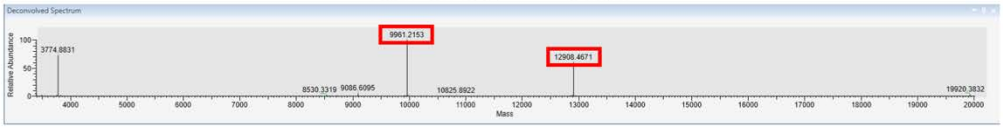

M. **PSL1_C37S**

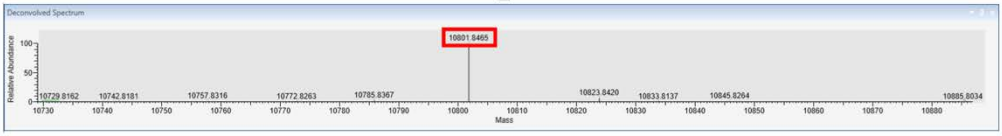

N. **PSL1_C37S reduced**

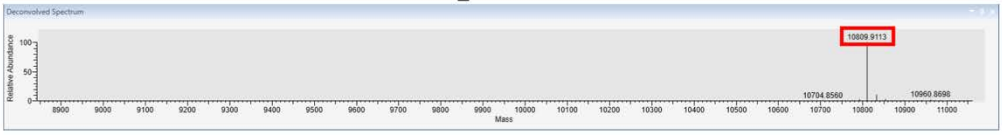

O. **SIX8_C58S**

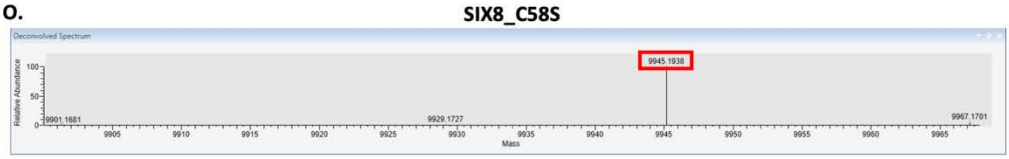

P. **SIX8_C58S reduced**

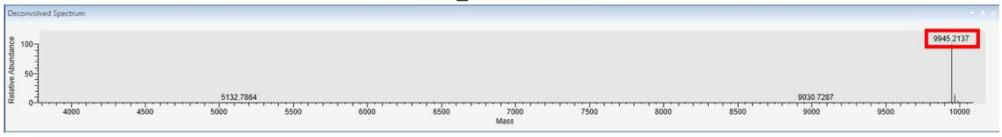

Q. **PSL1 + SIX8_C58S**

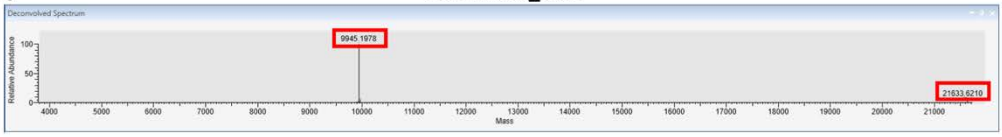

836

837

838

839

840

841

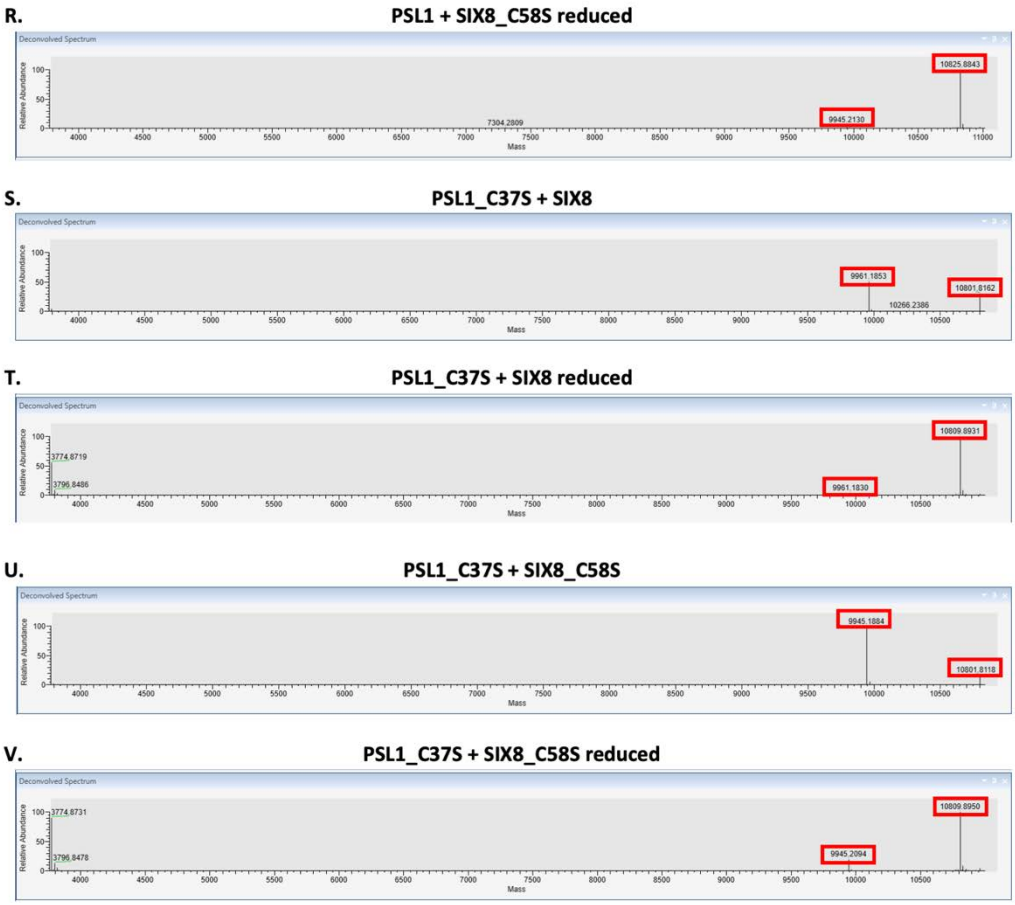

S9 Fig. Intact mass spectrometry analysis of the PSL1-SIX8 interaction. Deconvoluted mass spectra of **(A)** PSL1, **(B)** reduced PSL1, **(C)** SIX8, **(D)** reduced SIX8, **(E)** AvrSr50^{RKQQC}, **(F)** reduced AvrSr50^{RKQQC}, **(G)** PSL1 + SIX8, **(H)** reduced PSL1 + SIX8, **(I)** PSL1 + AvrSr50^{RKQQC}, **(J)** reduced PSL1 + AvrSr50^{RKQQC}, **(K)** SIX8 + AvrSr50^{RKQQC}, **(L)** reduced SIX8 + AvrSr50^{RKQQC}, **(M)** PSL1_C37S, **(N)** reduced PSL1_C37S, **(O)** SIX8_C58S, **(P)** reduced SIX8_C58S, **(Q)** PSL1 + SIX8_C58S, **(R)** reduced PSL1 + SIX8_C58S, **(S)** PSL1_C37S + SIX8, **(T)** reduced PSL1_C37S + SIX8, **(U)** PSL1_C37S + SIX8_C58S, **(V)** reduced PSL1_C37S + SIX8_C58S. Reduced samples were heated with DTT prior to running the samples.

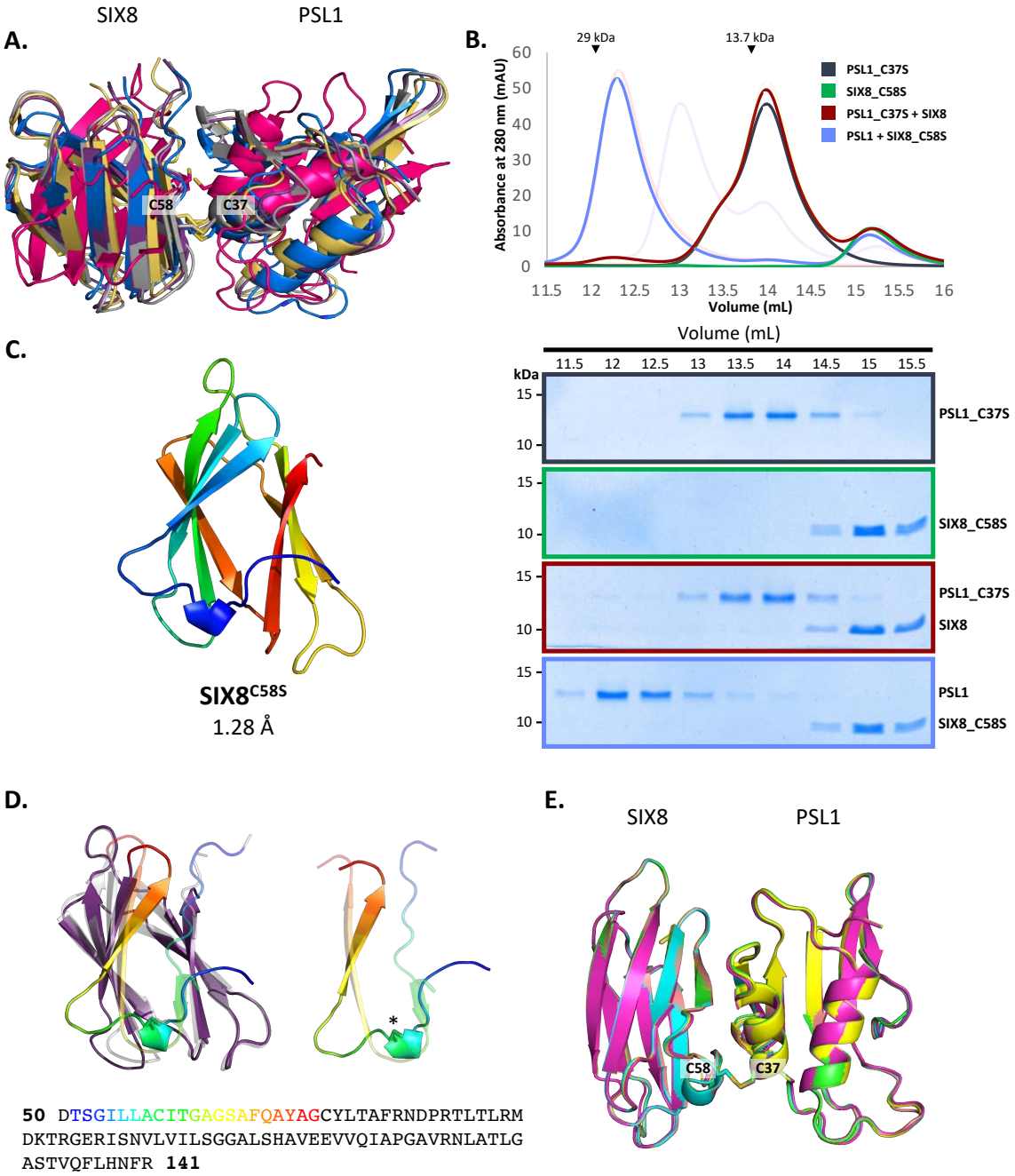

S10 Fig. Interaction between PSL1 and SIX8 mutants. (A) Model of the SIX8-PSL1 complex generated by AlphaFold2-Multimer (five models shown). Co-localisation of Cys 58 from SIX8 and Cys 37 from PSL1 shown in stick. **(B)** Size exclusion chromatograms of PSL1_C37S alone (black), SIX8_C58S alone (green), PSL1_C37S and SIX8 (maroon), and PSL1 and SIX8_C58S (light purple) following a 30 min incubation separated on a Superdex S75 Increase 10/300 SEC column (top panel). Equal concentrations of the protein were used (note the absorbance of SIX8 at 280 nm is ~0.3 resulting in a smaller absorbance and peak height). Indicated sizes above the chromatogram are based on protein standards run under similar conditions as presented in the manufacturer's column guidelines.

861 Transparent peaks correspond to the size exclusion chromatograms of PSL1 alone (red), SIX8 alone
862 (blue), PSL1 and SIX8 (purple) found in Figure 4B. Coomassie-stained SDS-PAGE gels depicting samples
863 taken from 500 µL fractions corresponding to the volumes indicated above the gels, with molecular
864 weights (left) and proteins (weight) annotated (bottom panel). **(C)** Cartoon representation of the
865 crystal structure of SIX8^{C58S} at 1.28 Å resolution, coloured from N (blue) to C (red) terminus. **(D)**
866 Comparison of the SIX8 structure and the AlphaFold2 model. The SIX8 structure (purple) and
867 AlphaFold2 model (grey) were superimposed using the DALI server (top panel) [33]. The N-terminus is
868 coloured in rainbow. The location of C58S is shown by an asterisk. Amino acid sequence of SIX8 with
869 residues of the N-terminus in rainbow corresponding to the structure (bottom panel). **(E)** Model of
870 the SIX8-PSL1 complex generated by AlphaFold2-Multimer (five models shown), when the SIX8^{C58S}
871 structure was used as a template. Co-localisation of Cys 58 from SIX8 and Cys 37 from PSL1 shown in
872 stick.
873

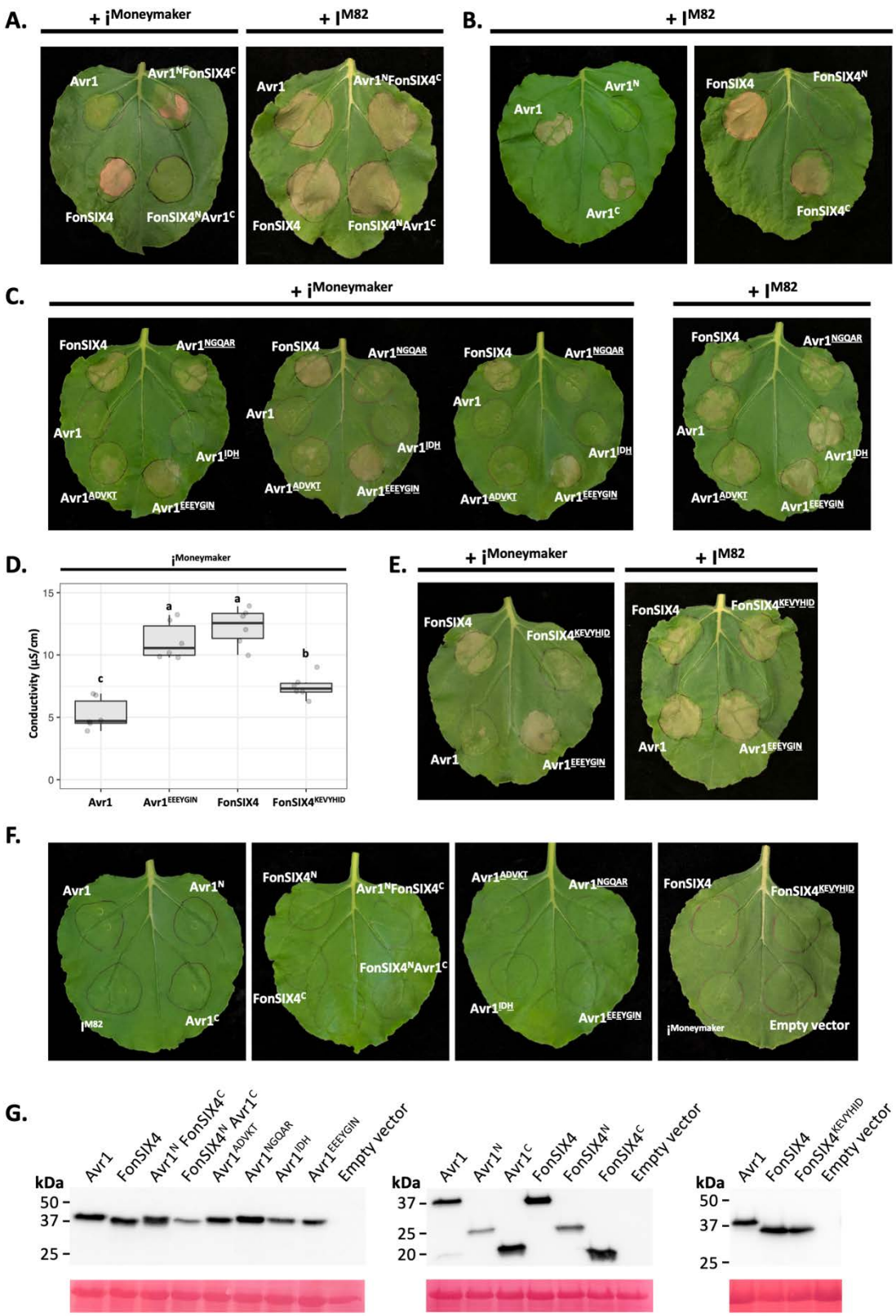

S11 Fig. (A) $i^{Moneymaker}$ recognises FonSIX4 at the C-domain. N and C-domain swapped chimeras of Avr1 and FonSIX4 were expressed with $i^{Moneymaker}$ (left panel) and I^{M82} (right panel). **(B)** The C-domains of Avr1 and FonSIX4 are sufficient for I^{M82} recognition. N and C-domains of Avr1 (left panel) and FonSIX4

878 (right panel) were expressed with I^{M82}. **(C)** Variation in the recognition response of Avr1 mutants by
879 $i^{Moneymaker}$. Avr1 mutants ($Avr1^{\underline{A}D\underline{V}K\underline{T}}$, $Avr1^{\underline{NGQAR}}$, $Avr1^{\underline{I}D\underline{H}}$, $Avr1^{\underline{E}E\underline{E}Y\underline{G}I\underline{N}}$) were co-expressed with $i^{Moneymaker}$
880 (left panel) or I^{M82} (right panel). **(D)** Ion leakage quantification of the reciprocal $Avr1^{\underline{E}F\underline{E}Y\underline{G}I\underline{N}}$ and
881 $FonSIX4^{\underline{K}E\underline{V}Y\underline{H}I\underline{D}}$ mutants when transiently co-expressed with $i^{Moneymaker}$. **(E)** Leaf images of $Avr1^{\underline{E}F\underline{E}Y\underline{G}I\underline{N}}$ and
882 $FonSIX4^{\underline{K}E\underline{V}Y\underline{H}I\underline{D}}$ mutants transiently co-expressed with $i^{Moneymaker}$ (left panel) or I^{M82} (right panel).
883 Polymorphic residues between Avr1 and FonSIX4 are underlined. **(F)** Effectors and receptors
884 expressed alone do not cause cell death in *N. benthamiana.* All Avr1, FonSIX4 effectors and I receptors
885 were transiently expressed in *N. benthamiana* via *Agrobacterium*-mediated transformation. Six
886 biological replicates were assessed for all qualitative assessment of I receptor mediated cell death in
887 *N. benthamiana*. All leaves were imaged 4 – 7 dpi. **(G)** Western blots of Avr1 and FonSIX4 constructs
888 with a C-terminal HA tag. Total proteins were extracted from *N. benthamiana* leaves 3 dpi and
889 separated by SDS-PAGE. The samples were transferred onto a membrane, probed anti-HA antibodies
890 and analysed under a chemiluminescence imager. The membrane was stained with Ponceau S to show
891 equal sample loading.

892

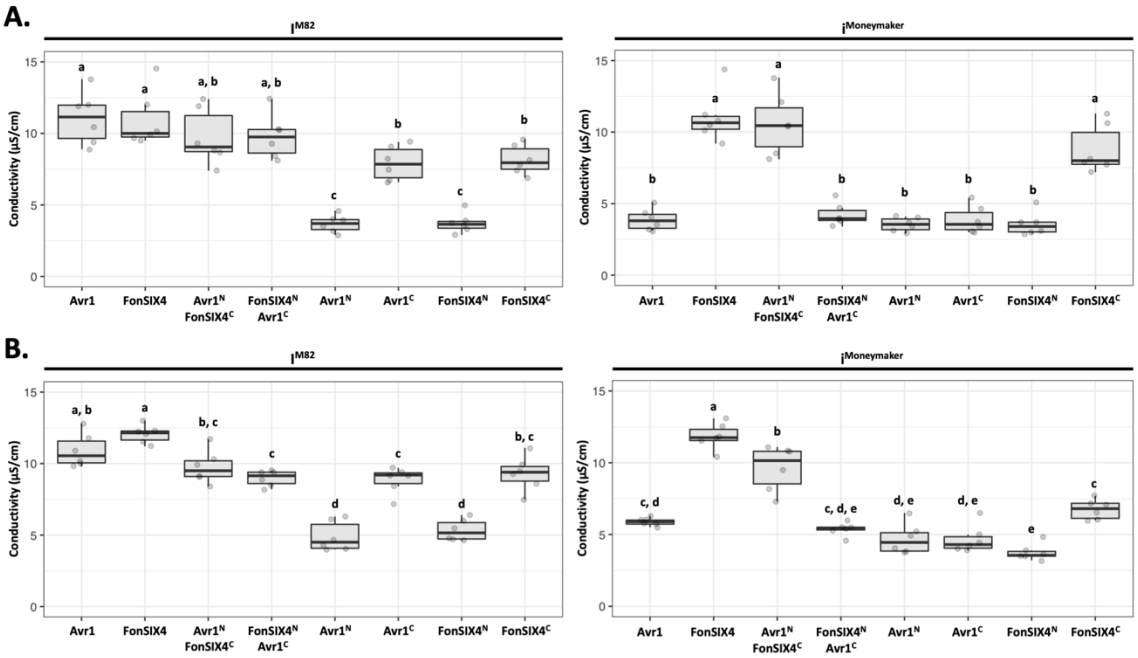

S12 Fig. A & B. Independent ion leakage experiments of different Avr1 and FonSIX4 constructs expressed with I^{M82} or $i^{Moneymaker}$. Avr1 and FonSIX4 effector constructs were transiently expressed with I^{M82} (left panels) or $i^{Moneymaker}$ (right panels) via *Agrobacterium*-mediated transformation in *N. benthamiana*. Six biological replicates each consisting of three leaf discs per leaf were harvested 24 hours post infiltration and incubated in water for 30 minutes. The water was replaced and the conductivity was measured after 24-48 hours. One-way ANOVA and post *hoc* Tukey's honestly significant difference tests were performed. Treatments that do not share a letter are significantly different from each other at $p < 0.05$.

```
SIX5     18  RDHQYCACQSGSGDSIDIDATTQLQNDNSKSYLWAQTSPAYWFADRHKPGPRFAGIYLKAA
SIX12    27  ---SSCLSVGPKGISNQNACVCGGQCVMKDLVVARR-----KVCCEYT-VQIQGGWPVLAQ
PSL1     18  EDWDRCRCMKYPETGTPNDCATIKACGSGKHRAISISEEKGDIWCEKTDVAISG--PEFY-
PSL2     18  EDWDQCRCMKYPSTGTPNDCATIKACGSGKHRAISIYKN-GDIWCEKTDVAING--PEFY-
SIX14    18  QRILGCRMPNGSLNPSPNICNQAGGSFRSGS----------RGCC--TRNTRDG--PVVTE

SIX5     79  NGKIDGDTFYNLCINNGGADSTCFDCSKSHQVRNVIYCDAA
SIX12    79  SRCVYGSTGA-----NGG--SCSGDNVSLAWWLNYEPEVKSTDPTCIFAKPKLCHS
PSL1     76  RTC-YGLLQD--PKPNSEADSCCTRWVDGVVVQSDGCFK
PSL2     75  RTC-YDLLQD--PKPNSEADSCCIKGDRA----SDGCFK
SIX14    65  SRFISGCNK------NGGFVSSKEILATSC
```

S13 Fig. Amino acid sequence alignment of SIX12 against Family 4 members reveals a similar cysteine spacing. All protein sequences have their signal peptides removed. The cysteine residues are highlighted in yellow and groups of two or more amino acid residues shared with SIX12 are highlighted in grey.

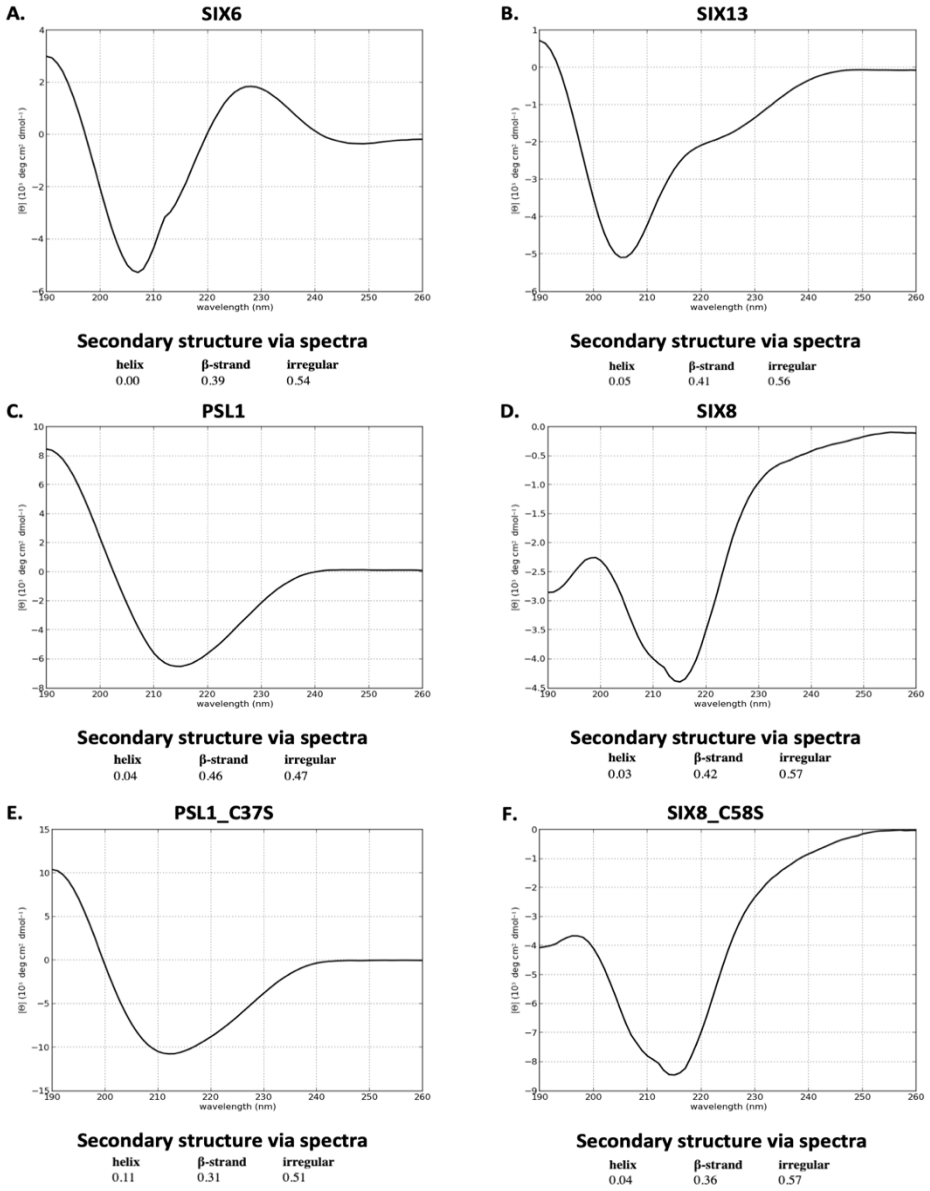

S14 Fig. Circular dichroism analysis of purified recombinant proteins. CD spectra of **(A)** SIX6, **(B)** SIX13, **(C)** PSL1, **(D)** SIX8, **(E)** PSL1_C37S and **(F)** SIX8_C58S proteins were plotted, and secondary structure elements analysed using the CAPITO webserver [81].

Supplementary tables

S1 Table. X-ray data collection, structure solution and refinement statistics for Avr1, Avr3, SIX6 and SIX8.

	Avr1 Bromide soak - SAD	**Avr1 Native (7T6A)**	**Avr3 Bromide soak - SAD**	**Avr3 Native (7T69)**	**SIX6 (8EBB)**	**SIX8 (8EB9)**
Detector	Dectris EIGER 2 9M	Dectris EIGER 16M	Dectris EIGER 2 9M	Dectris EIGER 16M	Dectris EIGER 2 9M	Dectris EIGER 16M
Wavelength (Å)	0.91946	0.95373	0.91969	0.95373	0.95336	0.95373
Space group	P1 21 1	P1 21 1	C2 2 21	C2 2 21	P 21 21 2	P43 2 2
Unit cell	69.87 38.24 80.10 90 103.56 90	70.00 40.34 81.30 90 104.54 90	54.68 79.93 117.12 90 90 90	54.86 80.13 117.37 90 90 90	76.303 93.544 60.489 90 90 90	51.814 51.814 81.599 90 90 90
Average mosaicity (°) [b]	0.00	0.08	0.00	0.06	0.06	0.05
Resolution (Å)	46.11 - 2.12 (2.18 - 2.12)	39.35 - 1.65 (1.68 - 1.65)	45.13 - 2.46 (2.56 - 2.46)	45.27 - 1.68 (1.71 - 1.68)	47.40-1.88 (1.92-1.88)	36.64-1.28 (1.326-1.28)
Total no. of reflections	1247183 (94443)	295538 (14086)	1426660 (157248)	280003 (13354)	243512 (15537)	381085 (37508)
No. of unique reflections	23868 (1868)	53375 (2645)	9668 (1079)	29849 (1458)	35252 (2205)	29449 (2869)
Completeness (%)	99.8 (98.1)	99.9 (100)	99.9 (99.4)	99.8 (96.8)	97.8 (96.8)	99.98 (99.97)
Multiplicity	52.3 (50.6)	5.5 (5.3)	147.6 (145.7)	9.4 (9.2)	6.9 (7.0)	13 (13)
Anomalous completeness	99.5 (96.8)	-	99.8 (98.7)	-		
Anomalous multiplicity	26.0 (25.2)	-	77.0 (75.3)	-		
Mean I /s(I)	24.0 (4.9)	13.1 (1.5)	25.1 (5.4)	14.5 (1.8)	11.8 (0.9)	23.71 (1.73)
Rmerge	0.157 (0.850)	0.074 (0.990)	0.215 (1.258)	0.072 (0.901)	0.070 (1.429)	0.048 (1.35)
Rmeas [c]	0.158 (0.858)	0.082 (1.010)	0.216 (1.262)	0.076 (0.953)	0.082 (1.668)	0.050 (1.41)
Rpim [d]	0.022 (0.117)	0.034 (0.470)	0.018 (0.102)	0.025 (0.308)	0.042 (0.857)	0.014 (0.39)
$CC_{1/2}$ [b]	0.999 (0.950)	0.999 (0.490)	1.0 (0.976)	0.999 (0.832)	0.999 (0.571)	0.999 (0.894)
Matthews coeff. ($Å^3$ Da^{-1}) [e]	2.60	2.78	2.13	2.13	2.82	2.56
Resolution range (Å)	-	39.35 - 1.65	-	45.27 - 1.68	46.77-1.88	36.64-1.28 (1.31-1.28)
R_{work} (%) [g]	-	16.85	-	16.88	19.32	17.0
R_{free} (%) [h]	-	21.10	-	21.77	22.10	19.33
No. of non-H atoms						
Total	-	3647	-	1882	2998	742
Macromolecules	-	3214	-	1713	2787	653
Ligand	-	20	-	10	20	5
Water	-	413	-	159	191	84
Average B-factor ($Å^2$)	-	26.06	-	28.27	40.73	23.79
RMSD from ideal geometry						
Bond lengths (Å)	-	0.005	-	0.012	0.008	0.011
Bond angles (°)	-	0.74	-	1.18	0.93	1.21
Ramachandran plot, residues in (%)[i]						
Favoured regions	-	97.77	-	95.57	98.58	98.85
Allowed regions	-	2.23	-	4.43	1.42	1.15
Outlier regions	-	0.00	-	0.00	0.00	0.00

[a] The values in parentheses are for the highest-resolution shell.
[b] Calculated with AIMLESS.
[c] Rmeas = $\Sigma_{hkl}\{N(hkl)/[N(hkl)-1]\}^{1/2}\ \Sigma i|Ii(hkl)-|/\ \Sigma hkl\Sigma iIi(hkl)$, where $Ii(hkl)$ is the intensity of the ith measurement of an equivalent reflection with indices hkl.
[d] Rpim = $\Sigma_{hkl}\{1/[N(hkl)-1]\}^{1/2}\ \Sigma i|Ii(hkl)-|/\ \Sigma hkl\Sigma iIi(hkl)$.
[e] Calculated with MATTHEWS_COEF within the CCP4 suite.
[f] Generated by Crank pipeline in the CCP4 suite.
[g] $R_{work} = \Sigma_{hkl}\ ||F_{obs}|-|F_{calc}||/\Sigma_{hkl}\ |F_{obs}|$, where F_{obs} and F_{calc} are the observed and calculated structure factor amplitudes.
[h] R_{free} is equivalent to R_{work} but calculated with reflections (5%) omitted from the refinement process.
[i] Calculated with MolProbity.

919 **S2 Table (supplementary file)**

920 **S3 Table.** Amino acid sequence inputs for AlphaFold2

Name	Sequence
SIX1$^{96-284}$	EPFGEESRNDRVTQDMLQALHDLCVERFGTGYRAVSGLCYTDRRATRKIECNKPSVRERDRSVTRACPKGQECTTFNAYNFRNRH HQVTFPVCGPRIEVKDRHDIGIHTEWQGTWYPESPKSPGTYDYFAQMAGTLNGYFGYDGVYSDGYKTSSHGYGHSWSCINCPRG KVTITNTYRATWAFGYTSPH
SIX2$^{98-221}$	GSCFSFPTPARGSCMIDYCWRDDNGVIYSRGITITGSNGASNPTSMRSNDPANLSLNSVFNDGYNGWFPHGHACSNSDTQIYTN HRLLQGVNGVAYVDHVRCENCNFRNVNCLSDVLKNNLIAYSNGVASQSRCT
SIX3$^{36-163}$	LPVEDADSSVGQLQGRGNPYCVFPGRPTSSTSFTTSFSTEPLGYARMLHRDPPYERAGNSGLNHRIYERSRVGGLRTVIDVAPPDG HQAIANYEIEVRRIPVATPNAAGDCFHTARLSTGSRGPATISWDADASYTYYLTISED
SIX4$^{59-242}$	SAHTESVCVHAGTATGADLHWLNAICTGKSTYTVNCAPAGNKNAGSTHTGTCPAGQDCFQLEQVGNFWGDREPDATCSPSNTV FDAVDDKEATHVNGKVVTRAGKPGIGRKLIRLKAQVYRRDGHYGQTSRMGFFRNGKEVYHIDNVASMEPTWNFDPSSDQSFSFF FTPGPNAFRIQGTLNLA
SIX5$^{18-119}$	RDHQYCACQSGSGDSIDIDATTQLQNDNSKSYLWAQTSPAYWFADRHKPGPRFAGIYLKAANGKIDGDTFYNLCINNGGADSTCF DCSKSHQVRNVIYCDAA
SIX6$^{58-225}$	DTLPVSTCPAGQKYDRSVCYKADKIRSFCVANPRSNREKITDTPCQPREICVQRNLSNGKSFAKCIPIVDLVEWKTSANGNKEGCTT TSVNPAGYHHLGTIVYDINKNPIEVDKISYFGEPGNVNEGIGGSTSYFSSDNFQFSKSRYMKTCIFSGGYGNLNAYTWSWE
SIX7$^{49-220}$	EVTFDITQNVNTFTSAASTPWTEGVGLSNIRYQWRAYYSTRQRTTFVEVRVFGTAEAQVVLLPDAPGTSRYRAIDSNVFRPNEEVT GGGLAGWGQVTTVCLQTWGRRGDITYRLRIQS
SIX8$^{50-141}$	DTSGILLACITGAGSAFQAYAGCYLTAFRNDPRTLTLRMDKTRGERISNVLVILSGGALSHAVEEVVQIAPGAVRNLATLGASTVQFL HNFR
SIX9$^{19-114}$	QTTQVGCRALDTKNDGLLTELLLNPSARGAADPDLRYGFWDAKWRKCCNKYKECDKYYTFSYNHPYPWAYRQRRGTIRGQQFDF ACVNWRTGACK
SIX10$^{15-149}$	IPDSGVSTGTKDLSKRDDAYIFDVTFRVGPAGANVAPFSGSVYVQDGLTPLVRSGSGSSISDRGYNAFRGIVYFTFTHGYNQYSAST RFGVYVDTGLIVDSNGRPIYGTAPRKACIDYSPHGPTDVCSVTITRSK
SIX11$^{19-110}$	INICCSSFAGHTCTKDQYNNHRQNVILNQIIDKDGVNCVRKGAGPGRWTRKGDWSEWYDCQQWNGPEQHQIEVGECTLFCVTP SGILNRPCI
SIX12$^{27-127}$	SSCLSVGPKGISNQNACVCGGQCVMKDLVVARRKVCCEYTVQIQGGWPVLAQSRCVYGSTGANGGSCSGDNVSLAWWLNYEP EVKSTDPTCIFAKPKLCHS
SIX13$^{78-293}$	QDDEHPNGPCPRGGRLYVDSDEDSSCNAKWGTQTHNDVKTFGSTGSVCAGTFRRITCACCYTMHPITDNNVPRMDGIYCPKWE VCKQEPERWSKWGNRVSHTSCVQAKKLTEILIATKKVVKEYCTPKRWLPSAGKGKNAKFHTWAYNYSTGQLTTLKWMYLKLDGQ YVKSAPGISEWGLTYSVNEHNAIELCGYPSDDMQRNSIDAELQWEATVQ
SIX14$^{18-88}$	QRILGCRMPNGSLNPSPNICNQAGGSFRSGSRGCCTRNTRDGPVVTESRFISGCNKNGGFVSSKEILATSC
PSL1$^{18-111}$ (FOXGR_025399)	EDWDRCRCMKYPETGTPNDCATIKACGSGKHRAISISEEKGDIWCEKTDVAISGPEFYRTCYGLLQDPKPNSEADSCCTRWVDGV VVQSDGCFK
FOXG_11033$^{24-226}$	APEAAPGYTTYGDYKGAGENLPSYPSYGSYGAKPKPKPKPAPAPKKYTNYGSYNYKKYSSYGHYKREAEPEAAPEAAPEAAPEAEA APGYTTYGDYKGAGENLPSYPSYGSYGSKPKPKPKPAPAPKKYTNYGSYNYKKYSSYGHYKREAEPEAAPEAEAEPETYSKYGSYPKK YTHYGSYNYKKYSSYGTYKRAKEFINSLF
FOXG_05755$^{56-157}$	NGVPDPGNFAASCHGLQVISDDLDLTGKPDFERCNDTAYEARQYFSGEYTTVEVRRTDYPDLGKEVQISATANYTSTNDNIVNGHL KFGDFQTKFISTPIEG
FOXG_18699$^{21-96}$	CKRTCSASNDAGTTCSYSCTQVCSSISAKQARDTFLAALQSGGNSCSAVGTSGVSCRKTAKFGSCYDHHWSCGSGC
FOXG_04863$^{106-300}$	MYDSSDDKGGLSDITRNAWSKFCNSPYGNNGGVTTRFILDGQWGAVGRLSGWSMRDALIHSMWQTADGIGKKNGYTVYNGC YGFTWQESKPGKANSACGGRSGKACPYNDDCPLAGMECTGLKWGTWMPSIIRMNVYNRDGSLRADAYQARISSQAVGSGGCS KAQTISAYVADFIPIVGPYFATGIRINCLYQS
FOXG_04805$^{39-132}$	QNGQNGGRPVPSGECCVANTSLKQDACTASNGQAGRCVPGGNNCGGRLSCVAQANLQCDANVIERGKDLCRAKAANGLFDG GNIIQNLSQAKVN
FOXG_02829$^{18-149}$	APSSPSDIQARSCVCKKVGDDWICTGTKCYDKVKRDLVPRQCSCHKIGDEWLCGGPKCPRDLPEENKLAKRQCSCHKVGDEWLC GGPKCPRSLPAEESGLEKRQCSCKKVAGEWICSGRKCPRDLSHLMGEE

FOXG_16600[17-164]	SPISKRAVFSQTTYDDLSISGGTAGNAQQEALQKLGGLPTDLSTVEKSDLDFLNSVNQIANDAEDEAFNPAIDAASGEAADALQRG KIKNKVLKLTATILKLQAQQAQGEDVADKLAEENKKLQNNISQDKDEAGKASTFLAFDATTS
FOXG_14684[38-168]	DGTCPRPMCTTPASQGPKDPPACGDSYAACKFDQFPCDEYFSPKVTDTHHCYCILANKKAMDAYCQERGFKSGTNPWKYYYAVE CHGAVSNQVCNKDCRDQGRGKGRIDKAHPNGACACDKPNPPYDTCKP
FOXGR_007323[18-86] *	SLVRRVDVNVPAMTNADGVVVPFDTAGVVQPAKKRDLEQKKRDLAQRKRHISRKRRAVSQEKQKQQQKQ
FOXGR_025639[18-61] *	APVVRGPGGRLVQEGAGCTLVQGRSVCDDGFGNTFFEDDPFSSK
PSL2[18-106] * (FOXGR_015322)	EDWDQCRCMKYPSTGTPNDCATIKACGSGKHRAISIYKNGDIWCEKTDVAINGPEFYRTCYDLLQDPKPNSEADSCCIKGDRASD GCFK
FOXGR_015533[19-114] *	QTCAIAPDPQRNADAFSATSHSGNIDIAFRDHVVFARPSAGTATGVLRLSNGDSYRKIYRIAGPNNVAQFYWLDASSQCKTNLAIT QMTNAAWYKE
FOXGR_015522[19-79] * (SIX15)	TIYCRDVSPPRDTRSWCKTNTPAWQGCQRFCSEHCRSTPRDYPDGCMYHLQVGGDYDCFCK

* Effector candidates identified in the reannotation of the *Fol* genome by Sun et al. (2022) and not predicted in the original genome annotation by Ma et al. (2010).

921

922

923 **S4 Table.** DNA sequences of synthesised gene fragments used in this study.

Name	Sequence (5' - 3')
SIX6*	TAGGTCTCCAATGGGTCCCTTAGCCCAAACAGAATCCGAGTCGGCAGACGTCGCTGAACATACAATCAATTATATCGACATTGCCCCTGAAGAATTTGAACCGCC CAAAGCTAATTTGTCATCTCTGGTGAGTCGTGACACGCTTCCTGTCAGTACCTGTCCTGCGGGTCAGAAATACGATCGTTCCGTGTGTTACAAGGCAGACAAAAT TCGTAGCTTTTGTGTCGCAAACCCTCGTAGCAACCGTGAGAAGATTACCGACACACCGTGTCAGCCCCGTGAAATCTGTGTGCAACGCAATCTTTCCAACGGCAA GAGTTTCGCTAAGTGTATCCCCATTGTAGACCTGGTGGAATGGAAGACATCCGCAAATGGGAATAAAGAAGGCTGTACTACAACGTCCGTGAATCCGGCTGGG TACCATCACCTTGGTACTATTGTTTACGATATCAATAAGAATCCTATCGAAGTTGATAAAATCTCGTACTTCGGCGAGCCGGGAAATGTAAACGAGGGCATTGGT GGCAGCACAAGCTATTTTAGTAGTGACAACTTTCAATTTTCTAAGTCCCGCTACATGAAAACTTGTATTTTCAGTGGTGGGTACGGGAATCTTAACGCCTATACGT GGAGCTGGGAATCTTGGAGACCGT
SIX6-TEV*	TAGGTCTCCAATGGGTCCCTTAGCCCAAACAGAATCCGAGTCGGCAGACGTCGCTGAACATACAATCAATTATATCGACATTGCCCCTGAAGAATTTGAACCGCC CAAAGCTAATTTGTCATCTCTGGTGGAAAATCTTTACTTCCAGTCCGACACGCTTCCTGTCAGTACCTGTCCTGCGGGTCAGAAATACGATCGTTCCGTGTGTTAC AAGGCAGACAAAATTCGTAGCTTTTGTGTCGCAAACCCTCGTAGCAACCGTGAGAAGATTACCGACACACCGTGTCAGCCCCGTGAAATCTGTGTGCAACGCAA TCTTTCCAACGGCAAGAGTTTCGCTAAGTGTATCCCCATTGTAGACCTGGTGGAATGGAAGACATCCGCAAATGGGAATAAAGAAGGCTGTACTACAACGTCCG TGAATCCGGCTGGGTACCATCACCTTGGTACTATTGTTTACGATATCAATAAGAATCCTATCGAAGTTGATAAAATCTCGTACTTCGGCGAGCCGGGAAATGTAA ACGAGGGCATTGGTGGCAGCACAAGCTATTTTAGTAGTGACAACTTTCAATTTTCTAAGTCCCGCTACATGAAAACTTGTATTTTCAGTGGTGGGTACGGGAATC TTAACGCCTATACGTGGAGCTGGGAATCTTGGAGACCGT
Avr1Thrombin*	TAGGTCTCCAATGTTGCCTAAAGGAGAGGAGGGTGACATTATTGGTACTTTCAATTTCTCGTCCAGCGACAGCCAACCCCTTAAAATCCACTGGGTCGATACGCC GGACTCATCTGGGAGCAATCTTGTTCCCCGTTCCGCTCACACGGAGAGTGTATGCGTTCACGCCGGGACCGCTACAGGTGCTGATCTGCATTGGTTGAATGCGA TCTGCACCGGGAAGTCTACATACACAGTGAATTGCGCCCCGGCAGGCAACAAGAATGCTGGGTCTACGCACACAGGAACATGTCCGGCAGGTCAGGACTGTTT CCAATTAGAGCAGGTCGGAAACTTTTGGGGGGACCGTGAGCCAGATGCTACCTGTAGCCCGTCCAATACGGTATTTGACGCCGTAGATGACAAGGAAGCTACG CATGTAAACGGCAAAGTTGTTACACGCGCGGGGAAGCCGGGCATTGGGCGCAAGCTTATTCGTCTTAAGGCTCAGGTCTATCGTCGTGATGGTCACTATGGTCA GACCTCGCGCATGGGATTCTTTCGTAACGGCAAAGAGGTTTACCATATCGACAACGTTGCCTCGATGGAACCCACTTGGAATTTTGACCCATCGAGTGACCAATC CTTTAGCTTCTTTTTCACACCGGGACCCAACGCTTTCCGTATTCAAGGAACGCTTAATCTGGCCTCTTGGAGACCGT
SIX8Thrombin*	TAGGTCTCCAATGACCCCGATTGACAAATCGTTAGATCAAGCGGCAACTATCGAAGAAACTGTCCACCAACCTCACTCCCATGATGAGCGTGCCTTAGTTCCACG TGGCAGCGATACGAGTGGGATTTTGCTGGCGTGTATTACCGGCGCAGGATCTGCGTTTCAGGCGTACGCTGGATGCTACTTAACAGCTTTCCGTAATGACCCTC GCACTTTAACTTTGCGTATGGATAAAACCCGTGGAGAACGTATTTCCAATGTTCTGGTTATCTTGTCAGGGGGTGCATTGAGTCACGCCGTGGAAGAAGTAGTAC AGATTGCGCCTGGAGCGGTCCGCAATTTGGCAACATTAGGAGCTTCGACTGTCCAATTCCTTCATAATTTTCGTTCTTGGAGACCGT
PSL1*	TAGGTCTCCAATGGAAGATTGGGATCGTTGTCGTTGCATGAAATACCCCGAAACTGGGACGCCGAATGACTGTGCCACCATTAAAGCGTGCGGTTCTGGCAAGC ACCGTGCCATCTCTATTTCGGAGGAGAAAGGAGACATTTGGTGCGAAAAGACTGATGTAGCAATCAGTGGACCGGAGTTCTACCGCACTTGCTATGGGTTGTTG CAGGACCCGAAGCCTAACTCGGAGGCAGATTCTTGTTGTACTCGTTGGGTAGACGGCGTTGTGGTACAATCTGACGGGTGCTTCAAATCTTGGAGACCGT
SIX13*	TAGGTCTCCAATGGAACTTGAAGTTTCCGATTTAAGTGATCAACCGCCGTCAGTGGAGAATACTTACCGCGACCAAGCGTTCAATGAGGAGGAGTTGTTAAAGG TCGTGGACGAATTATCCGTGGAGCGTACCGAACACACCGAACGCGCGCTTGTGAGTGAAGCGGCAGTCCAAAAGCGCCAGGACGACGAACATCCAAACGGTCC TTGTCCTCGCGGAGGACGTTTGTACGTGGATTCTGACGAAGACTCTTCTTGTAATGCGAAGTGGGGAACACAGACACATAACGATGTTAAGACTTTTGGCTCCAC CGGATCAGTCTGTGCCGGTACTTTTCGCCGCATTACGTGTGCTTGTTGTTACACGATGCATCCTATCACGGACAACAACGTTCCACGCATGGATGGTATTTACTGC CCTAAGTGGGAGGTGTGCAAACAAGAGCCTGAACGCTGGTCTAAGTGGGGCAATCGTGTAAGCCACACATCTTGCGTACAGGCGAAGAAGCTGACCGAAATCC TGATCGCTACTAAGAAAGTGGTGAAGGAATACTGCACCCCAAAACGTTGGTTACCATCTGCGGGAAAAGGCAAGAACGCGAAATTCCACACGTGGGCGTACAA TTATTCGACGGGTCAGCTTACAACCTTGAAGTGGATGTATTTGAAGTTGGACGGTCAGTATGTCAAGAGTGCGCCTGGGATCAGCGAGTGGGGGCTTACCTATT CAGTCAATGAACATAACGCGATTGAGTTATGTGGTTACCCAAGCGATGATATGCAACGCAATTCGATCGATGCTGAGCTTCAATGGGAGGCTACCGTACAGTCT TGGAGACCGT
SIX8_C58S Thrombin*	TAGGTCTCCAATGACCCCGATTGACAAATCGTTAGATCAAGCGGCAACTATCGAAGAAACTGTCCACCAACCTCACTCCCATGATGAGCGTGCCTTAGTTCCACG TGGCAGCGATACGAGTGGGATTTTGCTGGCGTCTATTACCGGCGCAGGATCTGCGTTTCAGGCGTACGCTGGATGCTACTTAACAGCTTTCCGTAATGACCCTCG CACTTTAACTTTGCGTATGGATAAAACCCGTGGAGAACGTATTTCCAATGTTCTGGTTATCTTGTCAGGGGGTGCATTGAGTCACGCCGTGGAAGAAGTAGTACA GATTGCGCCTGGAGCGGTCCGCAATTTGGCAACATTAGGAGCTTCGACTGTCCAATTCCTTCATAATTTTCGTTCTTGGAGACCGT
PSL1_C37S*	TAGGTCTCCAATGGAAGATTGGGATCGTTGTCGTTGCATGAAATACCCCGAAACTGGGACGCCGAATGACTCTGCCACCATTAAAGCGTGCGGTTCTGGCAAGC ACCGTGCCATCTCTATTTCGGAGGAGAAAGGAGACATTTGGTGCGAAAAGACTGATGTAGCAATCAGTGGACCGGAGTTCTACCGCACTTGCTATGGGTTGTTG CAGGACCCGAAGCCTAACTCGGAGGCAGATTCTTGTTGTACTCGTTGGGTAGACGGCGTTGTGGTACAATCTGACGGGTGCTTCAAATCTTGGAGACCGT
Avr1	ATCTTCTCACTCTACGCTTCCAAAGGGGGAGGAGGGTGACATCATCGGAACATTCAACTTTAGCAGCTCAGACAGTCAGCCGCTTAAAATCCACTGGGTAGATA CTCCGGATAGTTCAGGCTCCAATCTCGTTAAAAGATCTGCTCATACCGAGTCTGTTTGTGTACATGCTGGCACTGCTACTGGCGCAGATCTCCACTGGCTTAATGC AATATGCACTGGTAAATCGACATATACTGTTAACTGCGCGCCTGCGGGTAATAAAAATGCTGGATCGACACACACCGGAACATGTCCCGCAGGTCAGGATTGCT TCCAGTTGGAGCAAGTTGGCAACTTTTGGGGTGATAGAGAGCCTGACGCTACTTGCTCTCCGTCTAACACTGTTTTTGATGCGGTAGATGACAAGGAGGCAACA CATGTAAATGGCAAAGTTGTCACGCGTGCAGGAAAGCCAGGAATAGGACGAAAGCTCATTCGACTCAAGGCCCAAGTCTATCGCAGAGACGGGCATTATGGAC AAACTTCAAGAATGGGCTTTTTCCGTAATGGTAAGGAGGTATACCACATTGATAATGTGGCAAGCATGGAACCGACATGGAACTTTGATCCTTCCAGCGACCAG AGCTTTAGCTTCTTCTTCACTCCGGGGCCTAATGCATTTCGCATTCAAGGTACACTTAACTTAGCTTAGGTAATTTGGAGAGGA

Avr1^{ADVKT}

ATCTTCTCACTCTACGCTTCCAAAGGGGGAGGAGGGTGACATCATCGGAACATTCAACTTTAGCAGCTCAGACAGTCAGCCGCTTAAAATCCACTGGGTAGATA
CTCCGGATAGTTCAGGCTCCAATCTCGTTAAAAGATCTGCTCATACCGAGTCTGTTTGTGTACATGCTGGCACTGCTACTGGCGCAGATCTCCACTGGCTTAATGC
AATATGCACTGGTAAATCGACATATACTGTTAACTGCGCGCCTGCGGGTAATAAAAATGCTGGATCGACACACACCGGAACATGTCCCGCAGGTCAGGATTGCT
TCCAGTTGGAGCAAGTTGGCAACTTTTGGGGTGATAGAGAGCCTGACGCTACTTGCTCTCCGTCTAACACTGTTTTTGATGCGGCCGACGTGAAGACCGCAACA
CATGTAAATGGCAAAGTTGTCACGCGTGCAGGAAAGCCAGGAATAGGACGAAAGCTCATTCGACTCAAGGCCCAAGTCTATCGCAGAGACGGGCATTATGGAC
AAACTTCAAGAATGGGCTTTTTCCGTAATGGTAAGGAGGTATACCACATTGATAATGTGGCAAGCATGGAACCGACATGGAACTTTGATCCTTCCAGCGACCAG
AGCTTTAGCTTCTTCTTCACTCCGGGGCCTAATGCATTTCGCATTCAAGGTACACTTAACTTAGCTTAGGTAATTTGGAGAGGA

Avr1^{EEEYGIN}

ATCTTCTCACTCTACGCTTCCAAAGGGGGAGGAGGGTGACATCATCGGAACATTCAACTTTAGCAGCTCAGACAGTCAGCCGCTTAAAATCCACTGGGTAGATA
CTCCGGATAGTTCAGGCTCCAATCTCGTTAAAAGATCTGCTCATACCGAGTCTGTTTGTGTACATGCTGGCACTGCTACTGGCGCAGATCTCCACTGGCTTAATGC
AATATGCACTGGTAAATCGACATATACTGTTAACTGCGCGCCTGCGGGTAATAAAAATGCTGGATCGACACACACCGGAACATGTCCCGCAGGTCAGGATTGCT
TCCAGTTGGAGCAAGTTGGCAACTTTTGGGGTGATAGAGAGCCTGACGCTACTTGCTCTCCGTCTAACACTGTTTTTGATGCGGTAGATGACAAGGAGGCAACA
CATGTAAATGGCAAAGTTGTCACGCGTGCAGGAAAGCCAGGAATAGGACGAAAGCTCATTCGACTCAAGGCCCAAGTCTATCGCAGAGACGGGCATTATGGAC
AAACTTCAAGAATGGGCTTTTTCCGTAATGGTGAGGAAGAGTATGGTATTAACAATGTGGCAAGCATGGAACCGACATGGAACTTTGATCCTTCCAGCGACCAG
AGCTTTAGCTTCTTCTTCACTCCGGGGCCTAATGCATTTCGCATTCAAGGTACACTTAACTTAGCTTAGGTAATTTGGAGAGGA

Avr1^{IDH}

ATCTTCTCACTCTACGCTTCCAAAGGGGGAGGAGGGTGACATCATCGGAACATTCAACTTTAGCAGCTCAGACAGTCAGCCGCTTAAAATCCACTGGGTAGATA
CTCCGGATAGTTCAGGCTCCAATCTCGTTAAAAGATCTGCTCATACCGAGTCTGTTTGTGTACATGCTGGCACTGCTACTGGCGCAGATCTCCACTGGCTTAATGC
AATATGCACTGGTAAATCGACATATACTGTTAACTGCGCGCCTGCGGGTAATAAAAATGCTGGATCGACACACACCGGAACATGTCCCGCAGGTCAGGATTGCT
TCCAGTTGGAGCAAGTTGGCAACTTTTGGGGTGATAGAGAGCCTGACGCTACTTGCTCTCCGTCTAACACTGTTTTTGATGCGGTAGATGACAAGGAGGCAACA
CATGTAAATGGCAAAGTTGTCACGCGTGCAGGAAAGCCAGGAATAGGACGAAAGCTCATTCGACTCAAGGCCCAAGTCTATCGCAGAGACGGGCATTATGGAC
AAACTTCAAGAATGGGCTTTTTCCGTAATGGTAAGGAGGTATACCACATTGATAATGTGGCAAGCATGGAACCGACATGGAACTTTGATCCTTCGATTGATCACT
CGTTTAGCTTCTTCTTCACTCCGGGGCCTAATGCATTTCGCATTCAAGGTACACTTAACTTAGCTTAGGTAATTTGGAGAGGA

Avr1^{NGQAR}

ATCTTCTCACTCTACGCTTCCAAAGGGGGAGGAGGGTGACATCATCGGAACATTCAACTTTAGCAGCTCAGACAGTCAGCCGCTTAAAATCCACTGGGTAGATA
CTCCGGATAGTTCAGGCTCCAATCTCGTTAAAAGATCTGCTCATACCGAGTCTGTTTGTGTACATGCTGGCACTGCTACTGGCGCAGATCTCCACTGGCTTAATGC
AATATGCACTGGTAAATCGACATATACTGTTAACTGCGCGCCTGCGGGTAATAAAAATGCTGGATCGACACACACCGGAACATGTCCCGCAGGTCAGGATTGCT
TCCAGTTGGAGCAAGTTGGCAACTTTTGGGGTGATAGAGAGCCTGACGCTACTTGCTCTCCGTCTAACACTGTTTTTGATGCGGTAGATGACAAGGAGGCAACA
CATGTAAATGGCAAAGTTGTCACGCGTGCAGGAAAGCCAGGAATAGGACGAAAGCTCATTCGACTCAAGGCCCAAGTCTATCGCAGAGACGGGCATTATGGAC
AAACTTCAAGAATGGGCTTTTTCCGTAATGGTAAGGAGGTATACCACATTGATAATGTGGCAAGCATGGAACCGACATGGAACTTTGATCCTTCCAGCGACCAG
AGCTTTAGCTTCTTCTTCACTCCGGGGCCTAATGCATTTCGCATTCAAGGTACACTTAACTTAGCTTAGGTAATTTGGAGAGGA

FonSIX4

ATCTTCTCACTCTACGCTGCCGACCGATGAGGGGGATATTATCGGCACTTTTTCAATCGACAGTTCTGACTCACAGCCTATCAAGGTCCGCTGGTTAGATACGCCA
GAGATTTCTGGACGTTCGTTAGTCAAACGCTCGGCCTTGAGCCAGTCTGTCTGCACTCATGCTGGAACGGCGACGGGTGCCGATCTTCATTGGCTGAATGGGAT
TTGCACTGGGAAATCAACCTATACTGTGAATTGTGCTCCCGCAGGTAACAAAAATGCGGGGAGCTCCCACACCGGCACATGCCCACCGGACGAAGACTGTTTCC
AACTGGAGCGCGTGGGCAATTTCTGGGGCGACTTGGAACCCGATGTAACCTGTGCAAAGTCGGGCACAGTCTTTGACGCGGCCGACGTGAAGACCGCGACCCA
CGTTAACGGCAAAATTGTGACCCGTGCAGGAAAGCCTAACGGTCAGGCTCGCCTGATCCGCCTTAAAGCCCAAGTCTACCGCCGCGATGGTCATTATGGTCAGA
CCAGTCGCATGGGTTTCTTTCGTAACGGGGAGGAAGAGTATGGTATTAACAACGTGGCATCCATGGGGCCGACTTGGAATTTCGATCCTTCGATTGATCACTCGT
TCAGTTTCTTCTTCACGCCTGGGCCAGATGCATTCCGCGTACAGGGGACCATTAATTTAGCGTAGGTAATTTGGAGAGGA

FonSIX4^{KEVYHID}

ATCTTCTCACTCTACGCTGCCGACCGATGAGGGGGATATTATCGGCACTTTTTCAATCGACAGTTCTGACTCACAGCCTATCAAGGTCCGCTGGTTAGATACGCCA
GAGATTTCTGGACGTTCGTTAGTCAAACGCTCGGCCTTGAGCCAGTCTGTCTGCACTCATGCTGGAACGGCGACGGGTGCCGATCTTCATTGGCTGAATGGGAT
TTGCACTGGGAAATCAACCTATACTGTGAATTGTGCTCCCGCAGGTAACAAAAATGCGGGGAGCTCCCACACCGGCACATGCCCACCGGACGAAGACTGTTTCC
AACTGGAGCGCGTGGGCAATTTCTGGGGCGACTTGGAACCCGATGTAACCTGTGCAAAGTCGGGCACAGTCTTTGACGCGGCCGACGTGAAGACCGCGACCCA
CGTTAACGGCAAAATTGTGACCCGTGCAGGAAAGCCTAACGGTCAGGCTCGCCTGATCCGCCTTAAAGCCCAAGTCTACCGCCGCGATGGTCATTATGGTCAGA
CCAGTCGCATGGGTTTCTTTCGTAACGGGAAGGAGGTATACCACATTGATAACGTGGCATCCATGGGGCCGACTTGGAATTTCGATCCTTCGATTGATCACTCGT
TCAGTTTCTTCTTCACGCCTGGGCCAGATGCATTCCGCGTACAGGGGACCATTAATTTAGCGTAGGTAATTTGGAGAGGA

*Gene sequences have been codon optimised for expression in *E. coli*. Cloning overhangs have been underlined.

924

925 **S5 Table.** Primers used in this study

Name	Sequence (5'- 3')
Avr1_Fw	TAGGTCTCCAATGCTTCCAAAGGGGGAGGAGGGTG
Avr1_Rv	ACGGTCTCCAAGAAGCTAAGTTAAGTGTACCTTGAATGCGA
Avr3_Fw	TAGGTCTCCAATGCAAGAGGCTGCGGTTCGGGA
Avr3_Rv	ACGGTCTCCAAGAGGCGTTTGGATATACCAGCCCACAC
IF-Avr1_Fw	ATCTTCTCACTCTACGCTTCCAAAGGGGGAGG
IF-Avr1_Rv	TCCTCTCCAAATTACCTAAGCTAAGTTAAGTGTACCTTGA
IF-Avr1-Ctag_Rv	GCTTCCGCTAGCTAAGTTAA
IF-Avr1_3xHA_Fw	TTAGCTAGCGGAAGCTACCCATATGACGTTCCA
IF-Avr1-N_Rv	TCCTCTCCAAATTACCTACTAGTTAGACGGAGAGCAAGTAG
IF-Avr1-C_Fw	ATCTTCTCACTCTACGACTGTTTTTGATGCGGTAGAT
IF-Avr1-N-Ctag_Rv	GCTGTTAGACGGAGAGC
IF-Avr1-N_3xHA_Fw	TCTCCGTCTAACAGCTACCCATATGACGTTCCA
IF-FonSIX4_Fw	ATCTTCTCACTCTACGCTGCCGACCGATGAG
IF-FonSIX4_Rv	TCCTCTCCAAATTACCTACGCTAAATTAATGGTCCCC
IF-FonSIX4-Ctag_Rv	GCTTCCGCTCGCTAAATTA
IF-FonSIX4_3xHA_Fw	TTAGCGAGCGGAAGCTACCCATATGACGTTCCA
IF-FonSIX4-N_Rv	TCCTCTCCAAATTACCTACTAGCCCGACTTTGCACAGG
IF-FonSIX4-C_Fw	ATCTTCTCACTCTACGACAGTCTTTGACGCGG
IF-FonSIX4-N-Ctag_Rv	GCTGCCCGACTTTGC
IF-FonSIX4-N_3xHA_Fw	GCAAAGTCGGGCAGCTACCCATATGACGTTCCA
IF-3xHA_RvNew	TCCTCTCCAAATTACCTAGTAGTCAGGTACGTCGTAAG

926

927 **Literature Cited**

928 1. Dean R, Van Kan JAL, Pretorius ZA, Hammond-Kosack KE, Di Pietro A, Spanu PD, et al. The Top
929 10 fungal pathogens in molecular plant pathology. Mol Plant Pathol. 2012;13(4):414-430.
930 2. Rep M. Small proteins of plant-pathogenic fungi secreted during host colonization. FEMS
931 Microbiol Lett. 2005;253(1):19-27.
932 3. Houterman PM, Speijer D, Dekker HL, de Koster CG, Cornelissen BJC, Rep M. The mixed xylem
933 sap proteome of *Fusarium oxysporum*-infected tomato plants. Mol Plant Pathol. 2007;8(2):215-221.
934 4. Ma LJ, van der Does HC, Borkovich KA, Coleman JJ, Daboussi MJ, Di Pietro A, et al. Comparative
935 genomics reveals mobile pathogenicity chromosomes in *Fusarium*. Nature. 2010;464(7287):367-373.
936 5. Rep M, van der Does HC, Meijer M, van Wijk R, Houterman PM, Dekker HL, et al. A small,
937 cysteine-rich protein secreted by *Fusarium oxysporum* during colonization of xylem vessels is required
938 for *I-3*-mediated resistance in tomato. Mol Microbiol. 2004;53(5):1373-1383.
939 6. Schmidt SM, Houterman PM, Schreiver I, Ma L, Amyotte S, Chellappan B, et al. MITEs in the
940 promoters of effector genes allow prediction of novel virulence genes in *Fusarium oxysporum*. BMC
941 Genomics. 2013;14:119.
942 7. Vlaardingerbroek I, Beerens B, Rose L, Fokkens L, Cornelissen BJ, Rep M. Exchange of core
943 chromosomes and horizontal transfer of lineage-specific chromosomes in *Fusarium oxysporum*.
944 Environ Microbiol. 2016;18(11):3702-3713.
945 8. Gawehns F, Houterman PM, Ait Ichou F, Michielse CB, Hijdra M, Cornelissen BJC, et al. The
946 *Fusarium oxysporum* effector Six6 contributes to virulence and suppresses *I-2*-mediated cell death.
947 Mol Plant Microbe Interact. 2014;27(4):336-348.
948 9. Ma L, Houterman PM, Gawehns F, Cao L, Sillo F, Richter H, et al. The *AVR2-SIX5* gene pair is
949 required to activate *I-2*-mediated immunity in tomato. New Phytol. 2015;208(2):507-518.
950 10. van der Does HC, Lievens B, Claes L, Houterman PM, Cornelissen BJC, Rep M. The presence of
951 a virulence locus discriminates *Fusarium oxysporum* isolates causing tomato wilt from other isolates.
952 Environ Microbiol. 2008;10(6):1475-1485.
953 11. Gawehns F, Ma L, Bruning O, Houterman PM, Boeren S, Cornelissen BJC, et al. The effector
954 repertoire of *Fusarium oxysporum* determines the tomato xylem proteome composition following
955 infection. Front Plant Sci. 2015;6:967.
956 12. Li E, Wang G, Xiao J, Ling J, Yang Y, Xie B. A *SIX1* homolog in *Fusarium oxysporum* f. sp.
957 *conglutinans* is required for full virulence on cabbage. PLoS One. 2016;11(3):e0152273.
958 13. Thatcher LF, Gardiner DM, Kazan K, Manners JM. A highly conserved effector in *Fusarium*
959 *oxysporum* is required for full virulence on Arabidopsis. Mol Plant Microbe Interact. 2012;25(2):180-
960 190.
961 14. An B, Hou X, Guo Y, Zhao S, Luo H, He C, et al. The effector SIX8 is required for virulence of
962 *Fusarium oxysporum* f. sp. *cubense* tropical race 4 to Cavendish banana. Fungal Biol. 2019;123(5):423-
963 430.
964 15. Widinugraheni S, Nino-Sanchez J, van der Does HC, van Dam P, Garcia-Bastidas FA, Subandiyah
965 S, et al. A SIX1 homolog in *Fusarium oxysporum* f. sp. *cubense* tropical race 4 contributes to virulence
966 towards Cavendish banana. PLoS One. 2018;13(10):e0205896.
967 16. Cao L, Blekemolen MC, Tintor N, Cornelissen BJC, Takken FLW. The *Fusarium oxysporum* Avr2-
968 Six5 Effector Pair Alters Plasmodesmatal Exclusion Selectivity to Facilitate Cell-to-Cell Movement of
969 Avr2. Mol Plant. 2018;11(5):691-705.
970 17. Ayukawa Y, Asai S, Gan P, Tsushima A, Ichihashi Y, Shibata A, et al. A pair of effectors encoded
971 on a conditionally dispensable chromosome of *Fusarium oxysporum* suppress host-specific immunity.
972 Commun Biol. 2021;4(1):707.
973 18. Gonzalez-Cendales Y, Catanzariti AM, Baker B, McGrath DJ, Jones DA. Identification of *I-7*
974 expands the repertoire of genes for resistance to *Fusarium* wilt in tomato to three resistance gene
975 classes. Mol Plant Pathol. 2016;17(3):448-463.

19. Catanzariti AM, Do HTT, Bru P, de Sain M, Thatcher LF, Rep M, et al. The tomato *I* gene for *Fusarium* wilt resistance encodes an atypical leucine-rich repeat receptor-like protein whose function is nevertheless dependent on *SOBIR1* and *SERK3/BAK1*. Plant J. 2017;89(6):1195-1209.
20. Simons G, Groenendijk J, Wijbrandi J, Reijans M, Groenen J, Diergaarde P, et al. Dissection of the *Fusarium I-2* gene cluster in tomato reveals six homologs and one active gene copy. Plant Cell. 1998;10(6):1055-1068.
21. Catanzariti AM, Lim GTT, Jones DA. The tomato *I-3* gene: a novel gene for resistance to *Fusarium* wilt disease. New Phytol. 2015;207(1):106-118.
22. Houterman PM, Cornelissen BJC, Rep M. Suppression of plant resistance gene-based immunity by a fungal effector. PLoS Pathog. 2008;4(5):e1000061.
23. Houterman PM, Ma L, van Ooijen G, de Vroomen MJ, Cornelissen BJC, Takken FLW, et al. The effector protein Avr2 of the xylem-colonizing fungus *Fusarium oxysporum* activates the tomato resistance protein I-2 intracellularly. Plant J. 2009;58(6):970-978.
24. Di X, Cao L, Hughes RK, Tintor N, Banfield MJ, Takken FLW. Structure-function analysis of the *Fusarium oxysporum* Avr2 effector allows uncoupling of its immune-suppressing activity from recognition. New Phytol. 2017;216(3):897-914.
25. Sarma GN, Manning VA, Ciuffetti LM, Karplus PA. Structure of Ptr ToxA: an RGD-containing host-selective toxin from *Pyrenophora tritici-repentis*. Plant Cell. 2005;17(11):3190-3202.
26. Wang CI, Guncar G, Forwood JK, Teh T, Catanzariti AM, Lawrence GJ, et al. Crystal structures of flax rust avirulence proteins AvrL567-A and -D reveal details of the structural basis for flax disease resistance specificity. Plant Cell. 2007;19(9):2898-2912.
27. de Guillen K, Ortiz-Vallejo D, Gracy J, Fournier E, Kroj T, Padilla A. Structure analysis uncovers a highly diverse but structurally conserved effector family in phytopathogenic fungi. PLoS Pathog. 2015;11(10):e1005228.
28. Spanu PD. Cereal immunity against powdery mildews targets RNase-Like Proteins associated with Haustoria (RALPH) effectors evolved from a common ancestral gene. New Phytol. 2017;213(3):969-971.
29. Lazar N, Mesarich CH, Petit-Houdenot Y, Talbi N, Li de la Sierra-Gallay I, Zelie E, et al. A new family of structurally conserved fungal effectors displays epistatic interactions with plant resistance proteins. PLoS Pathog. 2022;18(7):e1010664.
30. Outram MA, Sung YC, Yu D, Dagvadorj B, Rima SA, Jones DA, et al. The crystal structure of SnTox3 from the necrotrophic fungus *Parastagonospora nodorum* reveals a unique effector fold and provides insight into Snn3 recognition and pro-domain protease processing of fungal effectors. New Phytol. 2021;231(6):2282-2296.
31. Outram MA, Solomon PS, Williams SJ. Pro-domain processing of fungal effector proteins from plant pathogens. PLoS Pathog. 2021;17(10):e1010000.
32. Yu D, Outram MA, Creen E, Smith A, Sung YC, Darma R, et al. Optimised production of disulfide-bonded fungal effectors in E. coli using CyDisCo and FunCyDisCo co-expression approaches. Mol Plant Microbe Interact. 2021.
33. Holm L. Dali server: structural unification of protein families. Nucleic Acids Research. 2022;50(W1):W210-W215.
34. Jumper J, Evans R, Pritzel A, Green T, Figurnov M, Ronneberger O, et al. Highly accurate protein structure prediction with AlphaFold. Nature. 2021;596:583-589.
35. Batson AM, Fokkens L, Rep M, du Toit LJ. Putative Effector Genes Distinguish Two Pathogenicity Groups of Fusarium oxysporum f. sp. spinaciae. Mol Plant Microbe Interact. 2021;34(2):141-156.
36. Czislowski E, Fraser-Smith S, Zander M, O'Neill WT, Meldrum RA, Tran-Nguyen LTT, et al. Investigation of the diversity of effector genes in the banana pathogen, Fusarium oxysporum f. sp. cubense, reveals evidence of horizontal gene transfer. Mol Plant Pathol. 2018;19(5):1155-1171.

1025 37. Lievens B, Houterman PM, Rep M. Effector gene screening allows unambiguous identification
1026 of Fusarium oxysporum f. sp. lycopersici races and discrimination from other formae speciales. FEMS
1027 Microbiol Lett. 2009;300(2):201-215.
1028 38. van Dam P, Fokkens L, Schmidt SM, Linmans JH, Kistler HC, Ma LJ, et al. Effector profiles
1029 distinguish formae speciales of Fusarium oxysporum. Environ Microbiol. 2016;18(11):4087-4102.
1030 39. Rocafort M, Bowen JK, Hassing B, Cox MP, McGreal B, de la Rosa S, et al. The *Venturia*
1031 *inaequalis* effector repertoire is dominated by expanded families with predicted structural similarity,
1032 but unrelated sequence, to avirulence proteins from other plant-pathogenic fungi. BMC Biology.
1033 2022;20(1):246.
1034 40. Varadi M, Anyango S, Deshpande M, Nair S, Natassia C, Yordanova G, et al. AlphaFold Protein
1035 Structure Database: massively expanding the structural coverage of protein-sequence space with
1036 high-accuracy models. Nucleic Acids Res. 2022;50(D1):D439-D444.
1037 41. van Kempen M, Kim SS, Tumescheit C, Mirdita M, Lee J, Gilchrist CLM, et al. Fast and accurate
1038 protein structure search with Foldseek. Nature Biotechnology. 2023.
1039 42. Iwaoka R, Nagata T, Tsuda K, Imai T, Okano H, Kobayashi N, et al. Structural insight into the
1040 recognition of r(UAG) by Musashi-1 RBD2, and construction of a model of Musashi-1 RBD1-2 bound to
1041 the minimum target RNA. Molecules. 2017;22(7):1207.
1042 43. Allen A, Chatt E, Smith TJ. The atomic structure of the virally encoded antifungal protein, KP6.
1043 J Mol Biol. 2013;425(3):609-621.
1044 44. Li J, Fokkens L, Conneely LJ, Rep M. Partial pathogenicity chromosomes in *Fusarium oxysporum*
1045 are sufficient to cause disease and can be horizontally transferred. Environ Microbiol.
1046 2020;22(12):4985-5004.
1047 45. Sun X, Fang X, Wang D, Jones DA, Ma L. Transcriptome Analysis of Fusarium-Tomato
1048 Interaction Based on an Updated Genome Annotation of Fusarium oxysporum f. sp. lycopersici
1049 Identifies Novel Effector Candidates That Suppress or Induce Cell Death in Nicotiana benthamiana. J
1050 Fungi (Basel). 2022;8(7).
1051 46. Evans R, O'Neill M, Pritzel A, Antropova N, Senior A, Green T, et al. Protein complex prediction
1052 with AlphaFold-Multimer. bioRxiv. 2022:2021.2010.2004.463034.
1053 47. Mirdita M, Schutze K, Moriwaki Y, Heo L, Ovchinnikov S, Steinegger M. ColabFold: making
1054 protein folding accessible to all. Nat Methods. 2022;19(6):679-682.
1055 48. Stergiopoulos I, de Wit PJGM. Fungal effector proteins. Annu Rev Phytopathol. 2009;47:233-
1056 263.
1057 49. Outram MA, Figueroa M, Sperschneider J, Williams SJ, Dodds PN. Seeing is believing:
1058 Exploiting advances in structural biology to understand and engineer plant immunity. Curr Opin Plant
1059 Biol. 2022;67:102210.
1060 50. Pennington HG, Jones R, Kwon S, Bonciani G, Thieron H, Chandler T, et al. The fungal
1061 ribonuclease-like effector protein CSEP0064/BEC1054 represses plant immunity and interferes with
1062 degradation of host ribosomal RNA. PLoS Pathog. 2019;15(3):e1007620.
1063 51. Pedersen C, Ver Loren van Themaat E, McGuffin LJ, Abbott JC, Burgis TA, Barton G, et al.
1064 Structure and evolution of barley powdery mildew effector candidates. BMC Genomics. 2012;13:694.
1065 52. Blondeau K, Blaise F, Graille M, Kale SD, Linglin J, Ollivier B, et al. Crystal structure of the
1066 effector AvrLm4-7 of *Leptosphaeria maculans* reveals insights into its translocation into plant cells and
1067 recognition by resistance proteins. Plant J. 2015;83(4):610-624.
1068 53. Petit-Houdenot Y, Langner T, Harant A, Win J, Kamoun S. A clone resource of *Magnaporthe*
1069 *oryzae* effectors that share sequence and structural similarities across host-specific lineages. Mol Plant
1070 Microbe Interact. 2020;33(8):1032-1035.
1071 54. Teulet A, Quan C, Evangelisti E, Wanke A, Yang W, Schornack S. A pathogen effector FOLD
1072 diversified in symbiotic fungi. New Phytol. 2023;239(3):1127-1139.
1073 55. Bauer S, Yu D, Lawson AW, Saur IML, Frantzeskakis L, Kracher B, et al. The leucine-rich repeats
1074 in allelic barley MLA immune receptors define specificity towards sequence-unrelated powdery

1075 mildew avirulence effectors with a predicted common RNase-like fold. PLoS Pathog.
1076 2021;17(2):e1009223.
1077 56. Seong K, Krasileva K. Computational structural genomics unravels common folds and novel
1078 families in the secretome of fungal phytopathogen *Magnaporthe oryzae*. Mol Plant Microbe Interact.
1079 2021.
1080 57. Yan X, Tang B, Ryder LS, MacLean D, Were VM, Eseola AB, et al. The transcriptional landscape
1081 of plant infection by the rice blast fungus Magnaporthe oryzae reveals distinct families of temporally
1082 co-regulated and structurally conserved effectors. Plant Cell. 2023;35(5):1360-1385.
1083 58. Seong K, Krasileva KV. Prediction of effector protein structures from fungal phytopathogens
1084 enables evolutionary analyses. Nat Microbiol. 2023;8(1):174-187.
1085 59. Ortiz D, Chen J, Outram MA, Saur IML, Upadhyaya NM, Mago R, et al. The stem rust effector
1086 protein AvrSr50 escapes Sr50 recognition by a substitution in a single surface-exposed residue. New
1087 Phytol. 2022;234(2):592-606.
1088 60. Park SY, Jeong MS, Park SA, Ha SC, Na BK, Jang SB. Structural basis of the cystein protease
1089 inhibitor *Clonorchis sinensis* Stefin-1. Biochem Biophys Res Commun. 2018;498(1):9-17.
1090 61. Renko M, Taler-Vercic A, Mihelic M, Zerovnik E, Turk D. Partial rotational lattice order-disorder
1091 in stefin B crystals. Acta Crystallogr D Biol Crystallogr. 2014;70(Pt 4):1015-1025.
1092 62. Dietrich JD, Longenecker KL, Wilson NS, Goess C, Panchal SC, Swann SL, et al. Development of
1093 orally efficacious allosteric inhibitors of TNFalpha via fragment-based drug design. J Med Chem.
1094 2021;64(1):417-429.
1095 63. Sulak O, Cioci G, Delia M, Lahmann M, Varrot A, Imberty A, et al. A TNF-like trimeric lectin
1096 domain from *Burkholderia cenocepacia* with specificity for fucosylated human histo-blood group
1097 antigens. Structure. 2010;18(1):59-72.
1098 64. Khoshnevis S, Neumann P, Ficner R. Crystal structure of the RNA recognition motif of yeast
1099 translation initiation factor eIF3b reveals differences to human eIF3b. PLoS One. 2010;5(9):e12784.
1100 65. Bull PC, Cox DW. Wilson disease and Menkes disease: new handles on heavy-metal transport.
1101 Trends Genet. 1994;10(7):246-252.
1102 66. Bleackley MR, Vasa S, Harvey PJ, Shafee TMA, Kerenga BK, Soares da Costa TP, et al. Histidine-
1103 rich defensins from the *Solanaceae* and *Brasicaceae* are antifungal and metal binding proteins. J Fungi
1104 2020;6(3):145.
1105 67. Lay FT, Ryan GF, Caria S, Phan TK, Veneer PK, White JA, et al. Structural and functional
1106 characterization of the membrane-permeabilizing activity of *Nicotiana occidentalis* defensin NoD173
1107 and protein engineering to enhance oncolysis. FASEB J. 2019;33(5):6470-6482.
1108 68. Prochnicka-Chalufour A, Corzo G, Satake H, Martin-Eauclaire MF, Murgia AR, Prestipino G, et
1109 al. Solution structure of discrepin, a new K+-channel blocking peptide from the alpha-KTx15 subfamily.
1110 Biochemistry. 2006;45(6):1795-1804.
1111 69. Korolkova YV, Bocharov EV, Angelo K, Maslennikov IV, Grinenko OV, Lipkin AV, et al. New
1112 binding site on common molecular scaffold provides HERG channel specificity of scorpion toxin BeKm-
1113 1. J Biol Chem. 2002;277(45):43104-43109.
1114 70. Van Duyne GD, Ghosh G, Maas WK, Sigler PB. Structure of the oligomerization and L-arginine
1115 binding domain of the arginine repressor of *Escherichia coli*. J Mol Biol. 1996;256(2):377-391.
1116 71. Cherney LT, Cherney MM, Garen CR, Lu GJ, James MN. Structure of the C-terminal domain of
1117 the arginine repressor protein from *Mycobacterium tuberculosis*. Acta Crystallogr D Biol Crystallogr.
1118 2008;64(Pt 9):950-956.
1119 72. Forderer A, Li E, Lawson AW, Deng YN, Sun Y, Logemann E, et al. A wheat resistosome defines
1120 common principles of immune receptor channels. Nature. 2022;610(7932):532-539.
1121 73. Ma S, Lapin D, Liu L, Sun Y, Song W, Zhang X, et al. Direct pathogen-induced assembly of an
1122 NLR immune receptor complex to form a holoenzyme. Science. 2020;370(6521):eabe3069.
1123 74. Martin R, Qi T, Zhang H, Liu F, King M, Toth C, et al. Structure of the activated ROQ1
1124 resistosome directly recognizing the pathogen effector XopQ. Science. 2020;370(6521):eabd9993.

1125 75. Plissonneau C, Daverdin G, Ollivier B, Blaise F, Degrave A, Fudal I, et al. A game of hide and
1126 seek between avirulence genes *AvrLm4-7* and *AvrLm3* in *Leptosphaeria maculans*. New Phytol.
1127 2016;209(4):1613-1624.
1128 76. Ghanbarnia K, Ma L, Larkan NJ, Haddadi P, Fernando WGD, Borhan MH. *Leptosphaeria*
1129 *maculans* AvrLm9: a new player in the game of hide and seek with AvrLm4-7. Mol Plant Pathol.
1130 2018;19(7):1754-1764.
1131 77. Haddadi P, Larkan NJ, Van deWouw A, Zhang Y, Xiang Neik T, Beynon E, et al. *Brassica napus*
1132 genes *Rlm4* and *Rlm7*, conferring resistance to *Leptosphaeria maculans*, are alleles of the *Rlm9* wall-
1133 associated kinase-like resistance locus. Plant Biotechnol J. 2022;20(7):1229-1231.
1134 78. Larkan NJ, Ma L, Haddadi P, Buchwaldt M, Parkin IAP, Djavaheri M, et al. The *Brassica napus*
1135 wall-associated kinase-like (WAKL) gene *Rlm9* provides race-specific blackleg resistance. Plant J.
1136 2020;104(4):892-900.
1137 79. Bentham AR, Youles M, Mendel MN, Varden FA, De la Concepcion JCB, Mark J. pOPIN-GG: A
1138 resource for modular assembly in protein expression vectors. bioRxiv. 2021:2021.2008.2010.455798.
1139 80. Iverson SV, Haddock TL, Beal J, Densmore DM. CIDAR MoClo: improved MoClo assembly
1140 standard and new *E. coli* part library enable rapid combinatorial design for synthetic and traditional
1141 biology. ACS Synth Biol. 2016;5(1):99-103.
1142 81. Wiedemann C, Bellstedt P, Gorlach M. CAPITO--a web server-based analysis and plotting tool
1143 for circular dichroism data. Bioinformatics. 2013;29(14):1750-1757.
1144 82. Cowieson NP, Aragao D, Clift M, Ericsson DJ, Gee C, Harrop SJ, et al. MX1: a bending-magnet
1145 crystallography beamline serving both chemical and macromolecular crystallography communities at
1146 the Australian Synchrotron. J Synchrotron Radiat. 2015;22(1):187-190.
1147 83. Kabsch W. *XDS*. Acta Crystallogr D Biol Crystallogr. 2010;66(Pt 2):125-132.
1148 84. Evans PR, Murshudov GN. How good are my data and what is the resolution? Acta Crystallogr
1149 D Biol Crystallogr. 2013;69(Pt 7):1204-1214.
1150 85. Winn MD, Ballard CC, Cowtan KD, Dodson EJ, Emsley P, Evans PR, et al. Overview of the *CCP4*
1151 suite and current developments. Acta Crystallogr D Biol Crystallogr. 2011;67(Pt 4):235-242.
1152 86. Skubak P, Pannu NS. Automatic protein structure solution from weak X-ray data. Nat
1153 Commun. 2013;4:2777.
1154 87. Skubak P, Arac D, Bowler MW, Correia AR, Hoelz A, Larsen S, et al. A new MR-SAD algorithm
1155 for the automatic building of protein models from low-resolution X-ray data and a poor starting model.
1156 IUCrJ. 2018;5(Pt 2):166-171.
1157 88. Afonine PV, Grosse-Kunstleve RW, Echols N, Headd JJ, Moriarty NW, Mustyakimov M, et al.
1158 Towards automated crystallographic structure refinement with *phenix.refine*. Acta Crystallogr D Biol
1159 Crystallogr. 2012;68(Pt 4):352-367.
1160 89. Emsley P, Lohkamp B, Scott WG, Cowtan K. Features and development of *COOT*. Acta
1161 Crystallogr D Biol Crystallogr. 2010;66(Pt 4):486-501.
1162 90. Aragao D, Aishima J, Cherukuvada H, Clarken R, Clift M, Cowieson NP, et al. MX2: a high-flux
1163 undulator microfocus beamline serving both the chemical and macromolecular crystallography
1164 communities at the Australian Synchrotron. J Synchrotron Radiat. 2018;25(Pt 3):885-891.
1165 91. Terwilliger TC, Grosse-Kunstleve RW, Afonine PV, Moriarty NW, Zwart PH, Hung LW, et al.
1166 Iterative model building, structure refinement and density modification with the *PHENIX AutoBuild*
1167 wizard. Acta Crystallogr D Biol Crystallogr. 2008;64(Pt 1):61-69.
1168 92. Almagro Armenteros JJ, Tsirigos KD, Sonderby CK, Petersen TN, Winther O, Brunak S, et al.
1169 SignalP 5.0 improves signal peptide predictions using deep neural networks. Nat Biotechnol.
1170 2019;37(4):420-423.
1171 93. Hellens RP, Edwards EA, Leyland NR, Bean S, Mullineaux PM. pGreen: a versatile and flexible
1172 binary Ti vector for *Agrobacterium*-mediated plant transformation. Plant Mol Biol. 2000;42(6):819-
1173 832.
1174 94. Stivala A, Wybrow M, Wirth A, Whisstock JC, Stuckey PJ. Automatic generation of protein
1175 structure cartoons with Pro-origami. Bioinformatics. 2011;27(23):3315-3316.

1176